主論文

Functional organization of segmentally homologous neurons in hindbrain

後脳分節間相同ニューロンの機能的構築

Daisuke Neki

根木　大輔

Division of Biological Science

Graduate School of Science

Nagoya University

This thesis is based on the following work:

Functional motifs composed of morphologically homologous neurons repeated in the hindbrain segment.

Daisuke Neki, Hisako Nakayama, Haruko Matsui-Frusho, Takashi Fujii, and Yoichi Oda

The Journal of Neuroscience, 2014, 34 (9): 3291-3302

Table of contents

Abstract

Repetitive neural structure, such as segments in the brainstem and columns in the neocortex, is a prominent feature of the central nervous system in vertebrates. At embryonic stages, the hindbrain develops as a series of visible neuroepithelial segments or rhombomeres, but there is no visible segmental anatomy in the adult brain of mammals or chicks. In a wide range of fishes, however, the adult hindbrain contains an orderly rhombomeric pattern of reticulospinal neurons (RSNs), individuals of which in goldfish and zebrafish are morphologically identified. It has been shown that RSNs sharing similar morphological features are repeated in adjacent segments and they are called segmental homologs. Despite the interesting arrangement of the RSNs, little is known about functional relationships among segmental homologs. We investigated electrophysiological connectivity between the Mauthner cell (M-cell), a pair of giant RSNs in segment 4 (r4) that are known to trigger fast escape behavior, and different series of homologous RSNs in r4–r6. This thesis consists of two parts.

(1) Morphological identifications of the segmentally homologous RSNs.

Intracellular recordings from the RSNs with a glass microelectrode filled with neurobiotin revealed the morphology of homologous RSNs in much more detail at the single cell level than the previous investigations. Principal features such as somatic location within the segment, axon pathway, and major dendritic arbors were highly conserved, whereas some minor differences in morphology were found among segmental homologous RSNs.

(2) Functional connectivity between the Mauthner cell and the segmentally homologous RSNs repeated in r4–r6.

Paired intracellular recordings in adult goldfish revealed unidirectional connections

from the M-cell to RSNs. The connectivities were found similar in morphological homologs: a single M-cell spike produced inhibitory postsynaptic potentials in dorsally located RSNs (MiD cells) on the ipsilateral side and excitatory postsynaptic depolarization on the contralateral side, except for MiD2cm cells. The inhibitory or excitatory potentials effectively decreased or enhanced target RSNs spiking, respectively. In contrast to the lateralized effects on MiD cells, single M-cell spiking elicited equally strong depolarizations on bilateral RSNs located ventrally (MiV cells), and the depolarization was high enough for MiV cells to burst.

Time course of synaptic potentials evoked by the M-cell firing and resulting effects on firing of each RSNs in r4–r6 suggest that each functional connection of a series of homologous RSNs from M-cell works as functional motifs during the M-cell-initiated escape. This study is the first to elucidate the intra-brainstem circuitry at the cellular level that controls the descending motor pathways in vertebrates.

General Introduction

Region-dependent functional and structural differentiations are observed in wide areas of the brain, and functional arrangement or organization has certain principles in each region. Repeated organization of unit structure or module is frequently found in the brain. Modules have been defined as a group of cells with the similar morphology, electrophysiological properties, or response properties (Leise, 1990). Considerable research efforts have been directed toward understanding the functional or modular organization of the brain such as the cortical columns (Mountcastle, 1957; Hubel and Wiesel, 1962), layer structure of neocortex (Mountcatle, 1997), cerebellum (Voogd and Glickstein, 1998), hippocampus (Supèr et al., 1998), tectum (Baier, 2013), olfactory glomerulus (Mori et al., 2006), the invertebrate optic lobes, and the antennal lobes (Strausfeld, 2009), because these structures may provide basic principles for the information processing in the brain or mechanisms underlying it.

The segmentation, which is one of the prominent features of brain structure, is comprised of repetition of a similar structural unit, segment, along the rostrocaudal axis. During early development, the vertebrate brain is comprised of the prosencephalon, mesencephalon, and rhombencephalon, which are then further segmentalized along the rostrocaudal axis (Lumsden and Keynes, 1989; Rubenstein et al., 1994). In the rhombencephalon, which is comprised of seven or eight segments, cranial motor neurons, RSNs, and vestibulospinal neurons are generated in a region-specific manner. From the earliest appearance of rhombomeres, each segment acquires the individual identity by expression of segment-specific genes, and

restriction of cell migration over the boundaries (Fraser et al., 1990; Terriente et al., 2012). In fish, from the primitive lamprey（Murakami et al., 2004） to teleost fishes including goldfish (Lee et al., 1993), zebrafish (Metcalfe et al., 1986), midshipman (Bass et al., 2008) and even evolutionary distant pufferfish (Greenwood et al., 2009), RSNs are periodically arranged orderly in the hindbrain segmental structure. Because RSNs project to the spinal cord, where they directly contact spinal interneurons or motoneurons, investigating RSNs is helpful to associate brain function with animal behaviors. RSNs are known to be involved in locomotion [walking, swimming, stopping the locomotion (Perrins et al., 2002), and prey tracking (Gahtan et al., 2005)], reaching (Schepens and Drew, 2004, 2006; Alstermark and Isa, 2012), and posture (Takakusaki et al., 1994; Deliagina et al., 2008). Further, some of the RSNs, which fire in relation to motor behaviors, are also active during rapid eye movement sleep (Thankachan et al., 2012). Locomotion is a critical capability of all vertebrate animals, and while there is accumulating data on descending pathways and spinal circuits (Kiehn, 2006; Grillner and Jessell, 2009; Fetcho and McLean, 2010), almost nothing is known about the intra-brainstem circuitry that modulates and organizes the descending motor pathways. In addition to the RSNs, T interneurons also show ladder-like arrangement in the larval zebrafish hindbrain (Kimmel et al., 1985). From these observations, it was proposed that the neurons of hindbrain reticular formation are segmentally organized (Kimmel et al., 1985). RSNs are morphologically identified in goldfish and zebrafish, and those that share common morphology, the time of appearance, and neurotransmitter, are repeated in adjacent segments (Mendelson, 1986b; Metcalfe et al., 1986; Lee et al., 1993; Kimura et al., 2013; Moly et al., 2014) and are called segmental homologs. In terms of cell position within the segment, axon pathway, and

dendritic feature, most RSNs are assigned to one of the major seven classes. Segmental repetition of reticular neurons sharing common axonal pathway is also observed in embryonic chick hindbrain (Clarke and Lumsden, 1993). Segments are hypothesized to arise from duplication of ancestral segment and therefore each segment or homologous neuron may also be related functionally with each other. However, it has remained to elucidate the functional organization of the segmentally homologous neurons (Metcalfe et al., 1986). Understanding of the RSNs functional organization may reveal functional networks controlling the behavior of animals.

The Mauthner cells (M-cells), a pair of giant RSNs in the 4th segment (r4), trigger fast escape (C-start) (Zottoli, 1977; Eaton et al., 1981) during initial phase of which the body is bent into a C-shape. The M-cells integrate various sensory inputs (Faber et al., 1989), elicit a single spike (Nakayama and Oda, 2004; Watanabe et al., 2014), and output onto spinal motorneurons and related interneurons (Fetcho and Faber, 1988; Satou et al., 2009) to initiate C-start by contracting the contralateral trunk muscle (Hackett and Faber, 1983a; Nissanov et al., 1990). However, a single M-cell spike is insufficient for entire escape, consisting of C-bend at stage 1 and subsequent propulsion at stage 2 (Eaton et al., 1988; Foreman and Eaton, 1993). Extracellular recordings in goldfish (Weiss et al., 2006) and Ca^{2+} imaging in zebrafish larvae (Gahtan et al., 2002) have suggested that other RSNs participate in C-starts, particularly segmental homologs of the M-cell, including paired MiD2cm in r5 and MiD3cm in r6 (the M-series) (O'Malley et al., 1996; Liu and Fetcho, 1999). M-series Ca^{2+} imaging revealed MiD2cm and MiD3cm are less activated during the M-cell-triggered escape (Kohashi and Oda, 2008), indicating functional relationships between the M-cell and its homologs. Two other

RSNs series in r4–r6 are also candidates: dorsally located, ipsilaterally projecting paired MiDi cells (MiM1 in r4, MiD2i in r5, and MiD3i in r6) and ventrally located, ipsilaterally projecting MiV cells (MiV1 in r4, MiV2 in r5, and MiV3 in r6), which are generated later than dorsal RSNs (Mendelson, 1986a, b) and form 8–18 neuronal clusters in hemisegments. Investigating the M-cell and homologous RSNs connectivity may reveal functional relationships of them in the M-cell-initiated escape.

The aim of present study is to approach the functional significance of the segmental structure by revealing the connections between the M-cell and other segmental homologous RSNs repeated in r4–r6, taking advantage of the features of identifiable goldfish RSNs. While zebrafish provide genetic and imaging advantages, the larger cells in goldfish allowed us to conduct paired recordings which are essential to mapping functional connections in intact neural networks. Although neurotransmission from the M-cell, which thought to be cholinergic, is blocked by bath-applied tubocurarine in zebrafish, that in goldfish is unblocked under the intramuscular injection of tubocurarine.

In this study, paired intracellular recordings of the M-cell and homologous RSNs in r4–r6 of adult goldfish revealed that there were unidirectional connections from the M-cells to RSNs and the connectivities were closely correlated with morphological homologies of the target neurons. These results would help us to understand functional significance of segmental homologs as well as fundamental escape network organized in the hindbrain segments.

Chapter 1

Morphological identification of the segmental homologous reticulospinal neurons in the adult goldfish hindbrain

Introduction

The RSNs are distributed from the midbrain to the medulla oblongata, or hindbrain, and the important interface between the higher brain centers and the cranial sensory systems on the one hand, and the spinal motor networks on the other in many vertebrates. The hindbrain RSNs are present in seven bilateral clusters (r1 to r7) that appeared periodically along neuraxis in larval zebrafish (Kimmel et al., 1982), in much the same way as segmented nervous system of the invertebrates. The segmental organization of RSNs was also shown in adult zebrafish (Lee and Eaton, 1991), juvenile goldfish (Lee et al., 1993), and adult goldfish (Nakayama and Oda, 2004). Each segment, separated by glial boundaries (Trevarrow et al., 1990; Heyman et al., 1995), contains individually identified RSNs. Twenty seven types of RSNs were identified in larval zebrafish (Metcalfe et al., 1986), twenty five types in adult zebrafish (Lee and Eaton, 1991), and thirty four types in juvenile goldfish (Lee et al., 1993). The RSNs, located in adjacent segments, often have similar morphological features as somatic location within each segment, gross dendritic morphologies and axonal pathway. They are referred to as the "segmental homologs" (Metcalfe et al., 1986). In addition to the morphological similarities, the segmental homologs share common developmental properties (Mendelson, 1986a, b). Segments are thought to have been derived from duplication and divergence on a long road of evolution (Metcalfe et al., 1986). To what extent is the morphology of homologous RSNs conserved?

In previous studies, the morphologies of RSNs were examined by backfilling of all RSNs through their axon in the spinal cord (Metcalfe et al., 1986; Lee et al., 1993). Here, I have conducted intracellular recordings from the RSNs with a glass microelectrode filled with neurobiotin to reveal the morphology of three series of homologous RSNs [M-series (M-cell in r4, MiD2cm in r5, and MiD3cm in r6), MiDi series (MiM1 in r4, MiD2i in r5, and MiD3i in r6), and MiV series (MiV1 in r4, MiV2 in r5, and MiV3 in r6)] much more detail at the single cell level than the previous investigations. In this chapter, we demonstrated gross anatomical structure of hindbrain RSNs in adult goldfish and then described morphologies of homologous RSNs in r4–r6 in detail.

Materials and Methods

Experiments were performed on adult goldfish of either sex (10–15 cm in length) at 20 °C. All procedures complied with the guidelines stipulated by the Committees on Animal Research of Nagoya University.

Intracellular recordings. During the experiment, fish were artificially respirated by gill perfusion with aerated water with 0.015% 3-aminobenzoic acid ethyl ester (MS222; Sigma) and immobilized with d-tubocurarine chloride (2 μg/mg body weight; Sigma). The skull was opened and the cerebellum was retracted rostrally to expose the medullar surface. Silver bipolar electrodes were placed just above the vertebral column for antidromic activation of the axons of RSNs. Intracellular recordings were obtained from the M-cells or other RSNs located in r4–r6 with an Axoprobe-1A preamplifier (Molecular Devices). A microelectrode was attached to a manipulator (ME-70, Narishige) placed on right side of the fish. In all trials, recording microelectrodes were filled with 4 M potassium acetate (5–10 MΩ at 60 Hz) containing 1.5%–5% neurobiotin (Vector

Laboratories) to label recorded neurons (Figure, 1). For locating RSNs, the axon cap of the M-cell, a neuropile surrounding the axon hillock and initial segment, was first located as a landmark with the help of an antidromically evoked large negative field potential (Figure 2A; Furshpan and Furukawa, 1962), as previously shown (Figure 3; Nakayama and Oda, 2004). This electrode was moved fixed distances three-dimensionally from the landmark (Figure 3), and RSNs were located with the help of field potentials of antidromic spikes evoked by spinal cord stimulation. The M-cells and other RSNs were electrophysiologically identified by antidromic spikes, evoked by stimulation of the caudal spinal cord (25–40 mm caudal to the recording sites), with short latencies of about 0.3 ms and 0.4–1.0 ms, respectively (Figure 2).

Intracellular labeling of RSNs. Recorded neurons were identified morphologically. To morphologically identify recorded neurons, neurobiotin was injected from the recording micropipette by passing iontophoretic anodal current pulses (20 nA) of 700 ms duration every 2 sec for 15 min. After the injection, the neurons were stained with an avidin–biotin complex (ABC) kit (Vector Laboratories) and visualized with 3′, 3′-diaminobenzidine, as described in a previous report (Nakayama and Oda, 2004). Labeled neurons were photographed with a digital CCD camera (Axiocam HRc; Zeiss) mounted on a light microscope (Axioskop; Zeiss) and reconstructed with camera lucida.

Results

Electrophysiological identification of RSNs

To examine the morphologies of RSNs, intracellular recordings were performed in adult goldfish. RSNs were electrophysiologically identified with antidromic action potential (AP) elicited by electrical stimulation at the spinal cord (Figures 2A, B) and

morphologically by their axonal pathway, location of somata and morphology of dendritic arbors labeled with neurobiotin (Figures 4, 5) (Lee et. al., 1993). All RSNs recorded in this study were silent at rest. Electrical stimulation elicited an antidromic AP in the M-cell and RSNs in an all-or-nothing manner at the threshold intensity.

The onset latency of antidromic AP elicited in the M-cell by the spinal stimulation applied at 25–40 mm caudal to the hindbrain was 0.29 ± 0.01 ms (range, 0.16–0.48, n = 45), which was significantly shorter than the latencies of other RSNs (0.6–0.8 ms; Figure 2C; $p < 0.001$, Mann–Whitney *U* test). The shortest latency of the M-cells among recorded RSNs demonstrated markedly fast conduction velocity in the M-cell axon (Table 1) and corresponded to the exceptionally large diameter of the myelinated M-axon.

Morphology of RSNs in r4–r6

In the present study, single intracellular labeling of recorded RSNs revealed morphological similarities and differences among the homologous neurons in more detail than that in a previous study that used retrograde labeling of the cells (Lee et al., 1993). RSNs were clearly identified as individuals, and the morphological features were highly reproducible among all animals we observed, as demonstrated in the previous studies (Kimmel et al., 1982; Metcalfe et al., 1986; Lee and Eaton, 1991; Lee et al., 1993; Gahtan et al., 2002; Gahtan and O'Malley, 2003). Locations of RSNs somata (Figure 3), determined by calculating the distance between the axon cap of M-cell and each RSN soma in reconstructed images, showed that RSNs were segmentally arranged along the rostrocaudal axis and that dorsally located MiD cells were separated from ventrally located MiV cells. The RSNs identified previously as homologous neurons shared

stereotypical similar morphology such as dorsoventral positions within the segment, the shapes of principal lateral and ventral dendrites, and axon paths into the spinal cord.

Pairs of dorsally located MiDcm and MiDi cells were repeated in r5 and r6 and had an axon that extended contralaterally and ipsilaterally, respectively. All MiD axons descended in the dorsal bundle of the medial longitudinal fasciculus (mlf_d) along the medial side of the M-axon as far as observed in the hindbrain. MiD cells showed one or sometimes two primary lateral dendrites and a few ventral dendrites extending dorsolaterally and rostroventrally, respectively. Furthermore, ventral dendrites extended rostrally beyond the boundary of the segment of their soma (Figures 4A–D) and approached the ventrolateral edge of the hindbrain (Figures 5A–C). MiD cells often exhibited another dendrite reaching the midline or further on the contralateral side (Figures 4A, 4C, 5A), which was not described in the previous study (Lee et al., 1993).

Ventrally located clusters, identified as MiV1, MiV2, and MiV3 cells in r4, r5, and r6, respectively, consisted of approximately 8–18 neurons. All MiV cells had an axon that descended ipsilaterally in the ventral medial longitudinal fasciculus (mlf_v) to the spinal cord, a thick lateral dendrite, and a few short ventral dendrites (Figures 4G, 4H, 4I, 5D, 5E, 5F), as observed in a previous report (Lee et al., 1993). In addition to the previously reported features, medial dendrites of MiV3 cells often crossed over the midline. Of interest, in some MiV3 cells (4 of 10 cells), a loop-shaped axon was observed: the axon first extended to the rostral border of r6 and then turned back to caudally descend to the spinal cord (Figure 4I). Furthermore, one MiV3 cell of 10 had a contralaterally descending axon in the mlf_v that branched from the ipsilateral main axon in the hindbrain.

In the present study, we found that MiM1 cells medioventrally located to the M-cell

soma in r4 were subdivided into two intermediate types: a pair of dorsally located MiM1 cells (denoted here as MiM1D cells) and probably a pair of ventrally located MiM1 cells (denoted here as MiM1V cells; Figures 4E, 4F, 6A). MiM1D cells were dorsally located (Figures 3, 6A, 6E) and have an ipsilateral descending axon, which projected to mlf_d (Figure 6B), similar to MiDi cells; however, MiM1D cells lacked lateral dendrite that directly dorsolaterally extended from the soma as MiD2i and MiD3i cells, and they instead possessed a thick bifurcated ventral dendrite that extend ventrally and then turned laterally (Figure 6A). MiM1V cells had an axon that descended in the ipsilateral mlf_v (Figure 6B) and lateral dendrites that were similar to those of more ventrally located MiV neurons in r4–r6 (Figure 6A). In addition, both MiM1D and MiM1V cells had a rostral dendrite that extended mediorostrally (Figures 4E, 4F). Therefore, MiM1D cells were morphologically similar to MiDi cells with some modifications, whereas MiM1V cells seemed to be rather similar to MiV cells.

Taken together, RSNs in r4–r6 were morphologically repeated, with some divergence such as the large soma of the M-cell among the M-series, the lack of a lateral dendrite in the MiM1D cells among the MiDi series, and the loop-shaped axon of the MiV3 cells among the MiV series.

Discussion

The morphological similarities and differences among the homologous RSNs in r4–r6 were confirmed by intracellularly labeling with neurobiotin. Segmentally arranged homologous RSNs, which could be identified by the single cell labeling technique, shared somatic location within the segment, axon pathway, and rough dendritic pattern. Morphological features of the dendrite and axon predict the input-output characteristics

of the RSNs.

Gross dendritic features of all MiD cells are similar to M-cell which have principle lateral and ventral dendrites, suggesting the possibility that they might receive inputs from auditory afferents on their lateral dendrites and visual inputs on their ventral dendrites. Their ventral dendrites may also connect to the torobulbar tract, and/or the medial lemniscus (Yamamoto et al., 2010) as well as tectobulbar tract (Bartelmez, 1915; Sharma et al., 1985; Zottoli et al., 1987; Sato et al., 2007). All MiV cells, which had a thick lateral dendrite at the ventral hindbrain, suggest that these cells also connect to the tectobulbar tract, the torobulbar tract, and/or the medial lemniscus. Axons of MiD and MiV cells run in the mlf_d and mlf_v, respectively. This different axonal pathway may be likely related to the topographic map that represents the speed/strength of movement along the dorsoventral axis (McLean et al., 2007; Fetcho and McLean, 2009).

Although principle morphological features (soma location within the segment, major dendritic shape, and axon pathway) were highly conserved among segmental homologous RSNs, some differences were found. Among M-series, only the M-cells were extraordinarily large cells, and MiD2cm cells had a medial dendrite that crossed the midline and bilaterally projecting axon branches (Gahtan and O'Malley, 2003). Among MiV series, only MiV3 cells sometimes had a loop-shaped axon and a medial dendrite that crossed the midline. These morphological differences in dendrites and axons imply functional differences among the homologous RSNs. In addition, I found two types of MiM1 cells (MiM1D and MiM1V) in r4. MiM1D, which was dorsally located and had an axon projecting ipsilateral mlf_d, was similar to MiDi cells, while MiM1V cells, which

was ventrally located and had an axon projecting ipsilateral mlf_v, was similar to MiV cells. These cells are interesting because they seem to embody the process of differentiation into dorsal RSN or ventral RSN.

M-series, MiDi series, and MiV series neurons output to the contralateral side of the dorsal spinal cord, ipsilateral side of the dorsal spinal cord, and ipsilateral side of the ventral spinal cord, respectively. RSNs which have a medial dendrite such as MiD2cm, MiD2i, and MiV3 cells integrate bilateral inputs and MiD2cm outputs to bilateral spinal cord.

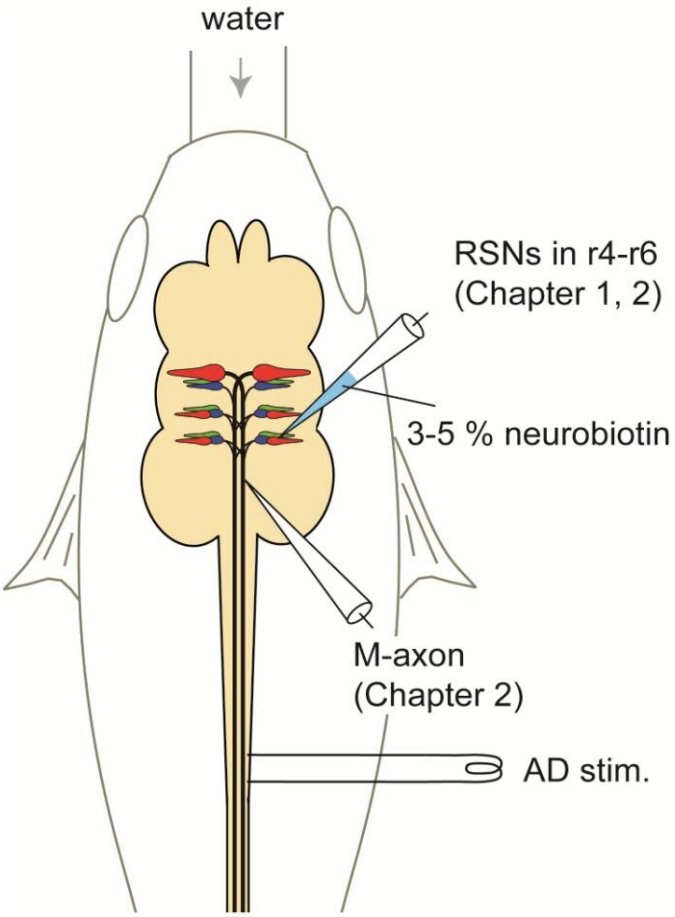

Figure 1. Schematic diagram indicates the experimental set-up. Fish were held horizontally in a recording chamber. Intracellular recordings were performed from somata of M-series neurons with glass micropipettes filled with 4M potassium acetate containing 3–5 % neurobiotin to label the recorded neurons (Chapter 1, 2). To activate an M-cell, another micropipette filled with 4 M KAc was inserted in the M-cell axon and depolarizing step currents were injected (Chapter 2). Bipolar stimulating electrodes were placed on the vertebral column for antidromic (AD) activation of the RSNs axons.

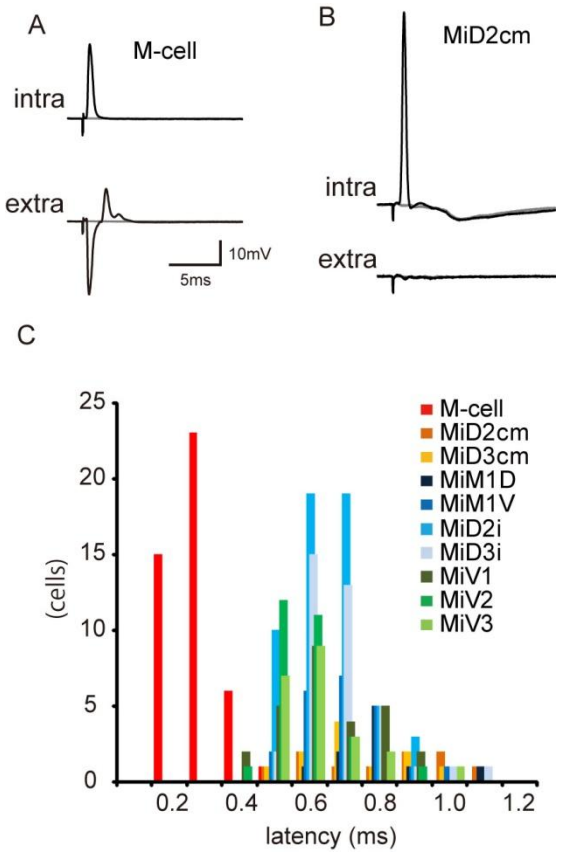

Figure 2. Electrophysiological identification of RSNs in r4–r6.

A and B: Antidromically evoked AP in the Mauthner cell (M-cell) (A) and a MiD2cm cell (B). Upper traces are intracellularly recorded APs (intra) that occurred in response to spinal cord stimulation at threshold intensities, and APs were observed in an all-or-nothing manner. Corresponding extracellular (extra) field potentials are shown below. Failures are represented by gray traces. Resting membrane potential (E_{rest}) was −80 mV in both the M-cell and MiD2cm cell. The calibration in A is also applicable to B. C: Frequency distribution of the onset latencies of antidromic spikes from spinal stimulation. The latencies of the M-cells (red) were distinctively shorter than those of other RSNs ($p < 0.001$, Mann–Whitney *U*-test): 0.29 ± 0.01 ms [mean ± standard error of the mean (SEM); range, 0.16–0.48; n = 45] in the M-cell, 0.68 ± 0.03 ms (n = 22) in MiD2cm, 0.58 ± 0.02 ms (n = 28) in MiD3cm, 0.82 ± 0.06 ms (n = 10) in MiM1D, 0.73 ± 0.04 ms (n = 11) in MiM1V, 0.64 ± 0.01 ms (n = 56) in MiD2i, 0.62 ± 0.03 ms (n = 22) in MiD3i, 0.81 ± 0.04 ms (n = 10) in MiV1, 0.63 ± 0.03 ms (n = 27) in MiV2, and 0.75 ± 0.02 ms (n = 20) in MiV3.

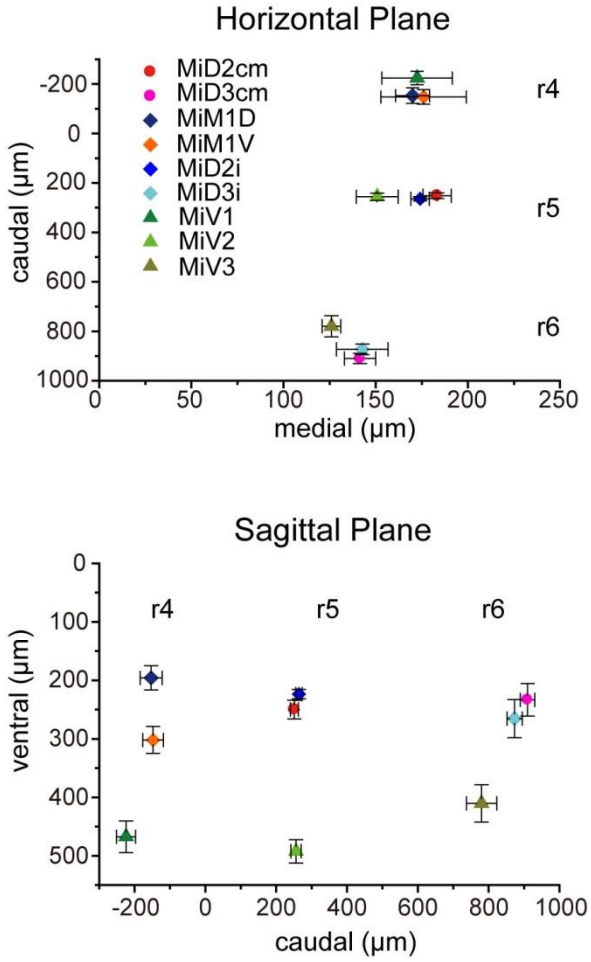

Figure 3. Positions of RSNs in r4–r6 as represented by three-dimensional distances from the axon cap of the Mauthner cell.

Caudomedial (upper) and ventrocaudal (lower) distances from the axon cap of the M-cell to the somata of intracellularly recorded RSNs. There were distinct spaces between RSNs in three segments (r4–r6) along the rostrocaudal and dorsoventral axes. MiD2cm cells (n = 15), MiD3cm cells (20), MiD2i cells (32), MiD3i cells (11), MiM1D cells (7), MiM1V cells (5), MiV1 cells (10), MiV2 cells (24), and MiV3 cells (10).

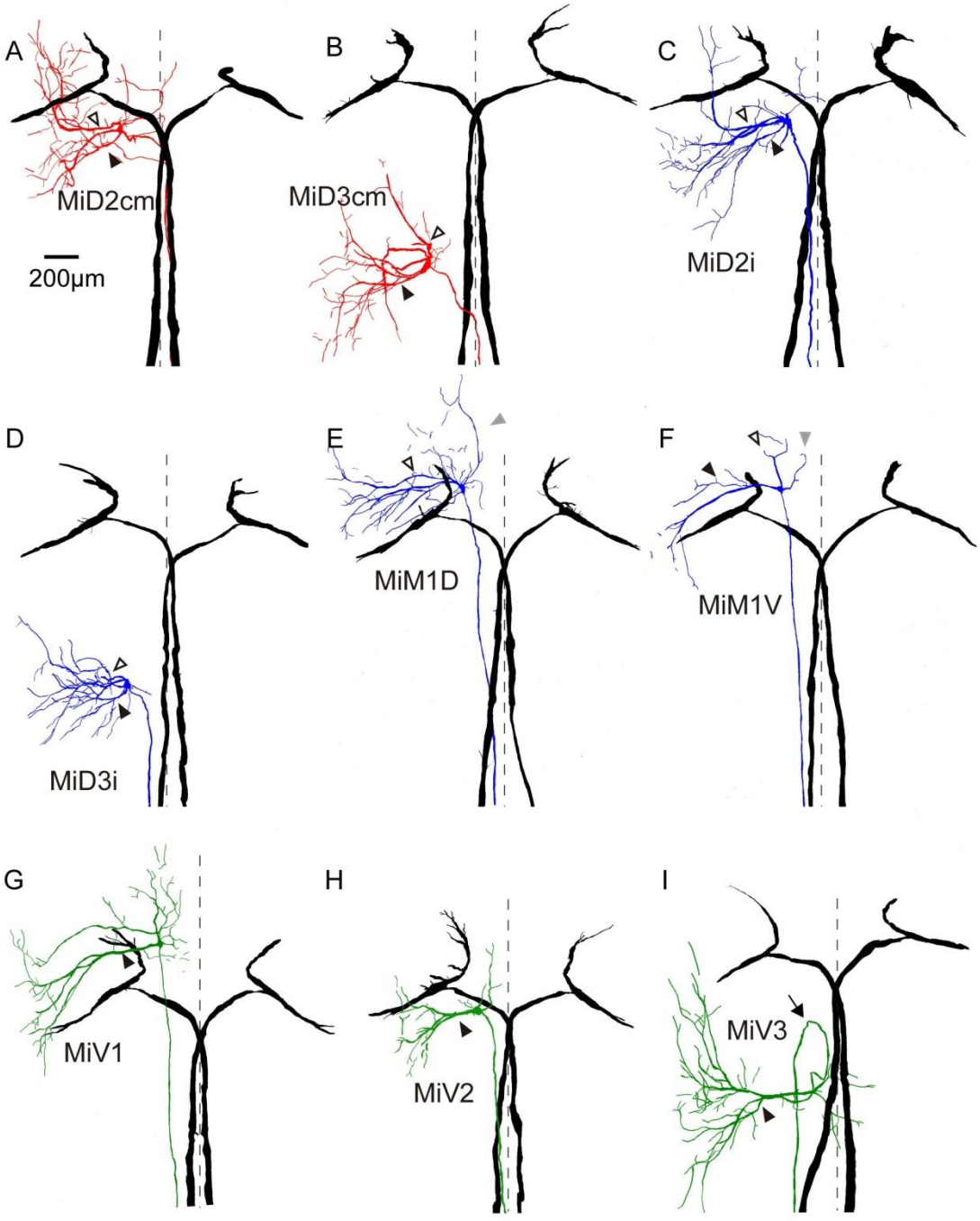
A
MiD2cm
200µm
B
MiD3cm
C
MiD2i
D
MiD3i
E
MiM1D
F
MiM1V
G
MiV1
H
MiV2
I
MiV3

Figure 4. Horizontally stacked images of the Mauthner cell and RSNs in r4–r6.
Camera lucida reconstructions from serial horizontal sections of paired, recorded, and intracellularly labeled the M-cells in r4 (black) and RSNs in r4–r6. The somata of all of types of RSNs fell into tidy segments, but their dendrites protruded away from their own segments and projected to the adjacent segments. A and B: Left MiD2cm cell in r5 (A) and MiD3cm cell in r6 (B) with bilateral M-cells. Both were located dorsally and had a stem axon that projected to the contralateral spinal cord as the M-cell. Broken lines indicate the midline (same in following traces of Figure 3 and 4). Filled arrowheads indicate the lateral dendrites, and open arrowheads indicate the ventral dendrites, which is the same in the following traces in Figures 3 and 4. C and D: MiD2i cell in r5 (C) and MiD3i cell in r6 (D), which had an axon that projected to the ipsilateral spinal cord. E and F: MiM1 cells in r4, of which an axon projected to the ipsilateral spinal cord, were subdivided into dorsally located MiM1D (E) and more ventrally located MiM1V cells (F): MiM1D cell possesses two main ventral dendrites that project ventrolaterally, and MiM1V cell possesses a large lateral dendrite. Both possess a rostral dendrite that projects rostroventrally (gray arrowheads). G–I: Ventrally located MiV1 cell in r4 (G), MiV2 cell in r5 (H), and MiV3 cell in r6 (I), which had an axon that projected to the ipsilateral spinal cord. These cells had a major thick lateral dendrite. Four of 10 MiV3 cells had an axon that projected rostrally and then caudally turned back (arrow). Up is rostral. The calibration in A is also applicable to B–I.

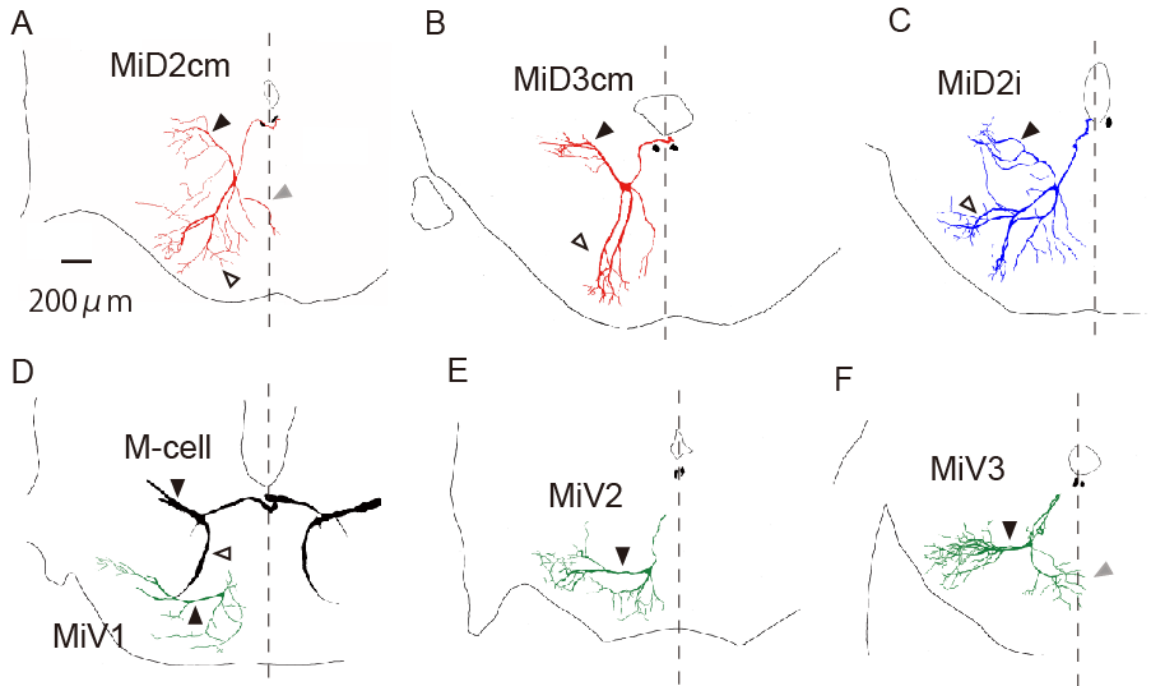

Figure 5. Frontally stacked images of RSNs in r4–r6.

Camera lucida reconstructions of rostral view from serial frontal sections of intracellularly labeled the M-cells (black) and other RSNs in r4–r6. A, B, C: The right MiD2cm cell in r5 (A), MiD3cm cell in r6 (B), and MiD2i (C) in r5 had an axon that dorsally projected to the dorsal bundle of the medial longitudinal fasciculus (mlf_d), where the M-axon extended. Sections of bilateral M-axons are shown in black. MiD2cm cell in r5 had a medial dendrite (gray arrowheads) that extended to the midline (broken lines). D–F: Ventrally located MiV1 cell in r4 (D), MiV2 cell in r5 (E), and MiV3 cell in r6 (F) had an axon projecting to the ventral bundle of the medial longitudinal fasciculus (mlf_v), which was located ventral to the M-axon. Dorsal is up. The calibration in A is also applicable to B–F.

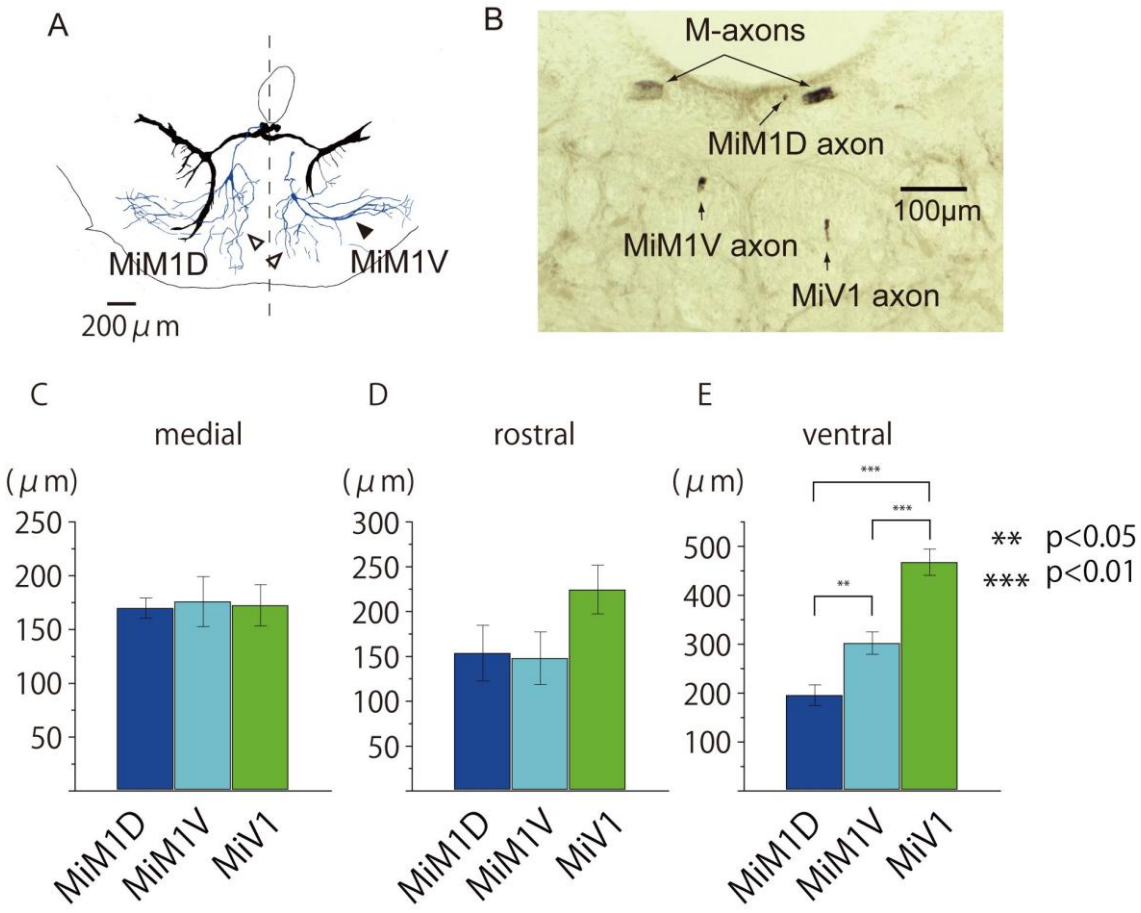

Figure. 6. Frontally stacked images and positions of MiM1D and MiM1V in r4.

Camera lucida reconstructions from serial frontal sections of intracellularly labeled the M-cells (black) and other RSNs in r4–r6. A: Simultaneous labeling of MiM1D (left) and MiM1V (right) cells with bilateral M-cells revealed the morphological differences of dendrites: the MiM1D cell possesses ventrally projecting bifurcated dendrites (open arrowhead), whereas the MiM1V cell possesses a thick lateral dendrite (filled arrowhead). H: A micrograph of the frontal section at the level of the caudal hindbrain. The MiM1D axon extended along with M-axons in the mlf_d, whereas MiM1V and MiV1 axons were located in dorsal and ventral mlf_v, respectively. C–E: Comparisons of the locations of RSNs in r4 segment. MiM1D, MiM1V, and MiV1 cells are located significantly different position along dorsoventral axis.

Table 1.

Conduction velocities (m/s) of axons of RSNs

	M-cell	MiD2cm	MiD3cm	MiM1D	MiM1V	MiD2i	MiD3i	MiV1	MiV2	MiV3
mean	117.3	48.3	52.4	44.7	47.6	50.7	47.5	44.8	51.2	39.1
SEM	3.2	1.4	1.5	3.8	2.9	0.9	1.5	2.6	1.2	1.0
n	45	22	28	10	11	56	22	10	27	20

Table 1. Conduction velocities (m/s) of axons of RSNs.

Values were calculated from the onset latency of the antidromic AP and the distance between the spinal stimulus site and the recording site in the hindbrain.

Chapter 2

Functional connectivity between the Mauthner cell and homologous reticulospinal neurons repeated in r4 to r6 in the goldfish hindbrain

Introduction

It has been thought that escape behavior is triggered by a single spike of an M-cell (Zottoli, 1977; Eaton et al., 1981, 1982, 1988; Hackett and Greenfield, 1986), however, an activation of the M-cell can reproduce only the initial part of the behavior (Nissanov et al., 1990). This implies that additional neurons acting along with or following the M-cell are needed to produce entire escape responses. Segmental homologous of the M-cell and other RSNs are suggested to be candidates working along with the M-cell during the escape from the previous calcium imaging study in larval zebrafish (O'Malley et al., 1996; Liu et al., 1999; Gahtan et al., 2002; Kohashi and Oda, 2008) and the observation that the M-series neurons can be excited by auditory inputs in parallel in adult goldfish (Nakayama and Oda, 2004). Actually, extracellular recordings of goldfish medulla oblongata during escape behavior revealed activation of other RSNs after the M-cell field potential (Weiss et al., 2006). In addition, Kohashi and Oda revealed complementary activation among M-series: MiD2cm and MiD3cm are activated during the escape in which the M-cell does not fire while less activated during the M-cell-triggered escape (Kohashi and Oda, 2008), indicating functional relationships between the M-cell and its homologs. So far, however, intra-brainstem functional connectivity during an M-cell-triggered escape was not known at all. In this chapter, functional connections between the M-cell and three series of segmental homologous RSNs in r4–r6 [M-series (MiD2cm in r5 and MiD3cm in r6), MiDi series

(MiM1 in r4, MiD2i in r5, and MiD3i in r6), and MiV series (MiV1 in r4, MiV2 in r5, and MiV3 in r6)] were examined by paired intracellular recordings.

Methods

For investigating synaptic connections between the M-cell and RSNs located in r4–r6, paired intracellular recordings were obtained from the M-cells and the RSNs with an Axoprobe-1A dual-channel preamplifier (Molecular Devices). Procedures for locating RSNs were the same in Chapter 1. After locating the RSN with one electrode, an M-cell axon was impaled with the other electrode at the level of the facial lobe.

To assess the synaptic connectivity between the M-cells and RSNs, one of the paired cells was activated by injecting stepwise depolarizing currents to elicit a single AP and voltage responses were recorded from the other. The latencies of the postsynaptic potentials (PSPs) were measured as the time between the peak of presynaptic AP and the onset of PSPs. In some experiments, strychnine (Sigma) was injected into the body musculature (5 μg/g body weight) to block glycinergic transmission. Electrophysiological data from RSNs with resting membrane potentials (E_{rest}) ranging from −70 to −91 mV were analyzed. Traces shown in the figures were the averages of 10–30 traces in PSPs without spiking, whereas the single traces in PSPs were with spiking. PSPs were represented as subtraction of the extracellular field potentials, which were obtained from the close vicinity of the cell just after intracellular recordings, from the intracellular membrane potentials.

Results

The M-cell outputs to ipsilateral MiD and MiM1D cells in r4–r6

Paired recordings of the M-cell and other RSNs revealed functional connectivity between them, which was closely related to morphological similarity. The M-cell AP elicited by intra-axonal depolarizing current pulses produced a biphasic postsynaptic response in the ipsilateral MiD cells, with an initial hyperpolarization followed by a slow prolonged depolarization (Figure 7). Homologous neurons showed similar amplitudes of hyperpolarizations at E_{rest}, and the amplitudes in MiDi were significantly smaller than those in MiDcm cells (Figure 7E). Furthermore, the time to peaks from the onset of IPSP were similar among these RSNs except for MiD2cm (Figure 7F). The hyperpolarizing responses were enlarged in amplitude when the MiD cells were depolarized by injecting anodal currents. The amplitude of responses was reduced by injecting hyperpolarizing current and was reversed in polarity by injecting stronger hyperpolarizing currents (Figures 7A–D), revealing that these hyperpolarizing responses were inhibitory postsynaptic potentials (IPSPs), with the reversal potential occurring near the E_{rest}. IPSPs were blocked by applying strychnine, indicating that they were mediated, at least in part, by glycinergic neurotransmission (Figure 7B below). Depolarizations persisted in strychnine. The onset latencies of IPSPs ranged from 1.0 to 1.2 ms (Table 2), suggesting chemically disynaptic inhibitory connections from the M-cell to these MiD cells. Because the M-cells are excitatory neurons and there was no morphological contact between the M-cell and ipsilateral RSNs, inhibitory interneurons were probably located in the pathways. IPSPs were followed by small depolarizations that lasted >200 ms (Figure 7G). In addition, in some recorded MiDi cells at r5 and r6, a sharp depolarizing potential with a short latency and small amplitude preceded IPSPs (Figures 7C, 7D below). The short latencies (0.6 ± 0.03 ms, n = 7 in MiD2i; 0.7 ± 0.12 ms, n = 3 in MiD3i) with a fast time course of their potential and

insensitivity to membrane polarization changes indicated that these components were mediated by gap junctions between MiDi cells and presynaptic interneurons that were innervated by the M-axon. With regard to MiM1D cells in r4, which are probably homologous to MiDi cells in r5 and r6, the M-cell delivered IPSPs to the ipsilateral MiM1D cell with a latency of 1.0 ms (n = 3), similar to ipsilateral MiD cells in r5 and r6 (Figure 9A).

These results demonstrated that disynaptic inhibitory connections from the M-cell to ipsilateral dorsally located RSNs were repeated in the adjacent segments (r4–r6) with a preceding small excitation in some MiDi cells.

The M-cell outputs to contralateral MiD and MiM1D cells in r4–r6

In contrast to ipsilateral MiD and MiM1D cells, long-lasting (>200 ms) depolarizations were elicited in the contralateral MiD (Figure 8B–D) and MiM1D (Figure 9B) cells in r4–r6. The onset latencies of the responses (Table 2) suggested that they were mediated by di- or polysynaptic pathways from the M-cell. A short hyperpolarization with latency of 2.0 ± 0.05 ms (n = 6) was evoked in MiD2cm only, and it was followed by a slow depolarization (Figure 8A), similar to ipsilateral MiD2cm. The depolarizations in MiDi cells were similar in shape, and peak time from the onset was significantly shorter than that in MiD3cm cells (Figures 8E, F).

Thus, the connectivity from the M-cell to contralateral MiD and MiM1D cells was excitatory and contrasted to that of the ipsilateral MiD cells, and these excitatory connections were similar (duplicated) in r4–r6, with the exception of MiD2cm.

The M-cell outputs to MiV cells in r4–r6 and MiM1V cells in r4

In stark contrast to dorsally located MiD cells, strong excitation was elicited in ventrally located MiV cells in r4–r6 on both sides by M-cell firing. A single AP of the M-cell produced bursts of bilateral MiV1, MiV2, and MiV3 cells (Figure 10). The underlying PSPs, which were observed by hyperpolarizing the recorded cells (Figures 10C, D, lower traces), showed onset latencies that ranged from 0.9 to 1.5 ms (Table 2), indicating disynaptic excitatory connections from the M-cell to MiV cells in r4–r6. The symmetrical strong excitatory connectivity from the M-cell to MiV cells was repeated through r4–r6. However, there was a modification in the connectivity to MiV2 cells. Long-lasting depolarizations were observed in MiV2 cells in r5 (Figures 10C, D), whereas hyperpolarization followed after initial depolarization in MiV1 cells in r4 and MiV3 cells in r6 (Figures 10A, B, E, F).

In addition, the M-cell also provided symmetrical excitation to bilateral MiM1V cells, but it was not enough to elicit spiking (Figures 9C, D), supporting the idea that MiM1 cells were also functionally segregated into MiDi-type MiM1D cells and MiV-type MiM1V cells with respect to the connectivity with the M-cell.

Single spiking of the M-cell was strong enough to suppress or increase the firing activity of MiD and MiV cells

RSNs are thought to be involved in various motor activities, including escape (O'Malley et al., 1996; Gahtan et al., 2002; Weiss et al., 2006; Kohashi and Oda, 2008), optomotor response (Orger et al., 2008; Huang et al., 2013), swimming (Ahrens et al., 2013; Kimura et al., 2013), and hatching (Eaton et al., 1977). Next we determined where and how spiking of these RSNs was effectively modified when the M-cell was fired to initiate fast escape. To examine this, we assessed the effects of the M-cell firing on spiking in

RSNs elicited by intracellular injections of depolarizing current (Figure 11). Repetitive firing of MiD cells (Nakayama and Oda, 2004) was suppressed for approximately 10–50 ms, and this was followed by brief rebound excitation after a single AP of the ipsilateral M-cell (Figures 11A–D). The duration of spike suppression depended on the firing frequency of RSNs before the M-cell spike (Figure 11C), but spiking was definitely blocked for at least 8 ms after the M-cell firing. In contrast, spiking of MiD3cm, MiD2i, and MiD3i cells on the contralateral side was intensively enhanced for approximately 10 ms after a single AP of the M-cell (Figure 11D, right) and slightly for the following long period. Thus, the M-cell sends bilateral asymmetrical outputs to dorsally located MiD cells, except for MiD2cm, to which there are symmetrical inhibitory outputs, as expected from PSPs elicited by the M-cell. In contrast, the activation of the M-cell exerted a strong impact on bilateral MiV cells, inducing an initial burst at an extremely high frequency (up to 300–500 Hz) in r4–r6 MiV cells with subsequent moderate, long-lasting enhancements of spiking in MiV2 cells (Figures 11E, F) or strong suppression in MiV1 and MiV3 cells (Figures 11G, H).

Together with these effects on RSNs in r4–r6, these findings suggested that when one of the paired M-cell was fired to initiate escape, spiking activation was transiently suppressed in ipsilateral MiD cells and moderately facilitated in contralateral MiD cells, with the exception of MiD2cm cells. In contrast, MiV cells located on both sides in r4–r6 received symmetrical and long-lasting effects.

No inputs from RSNs to the M-cell

All of these data showed that there were functionally effective connections from the M-cell to RSNs in r4–r6. We next aimed to determine whether there are functional

connections in the reciprocal direction, by recording from the M-cell while evoking spikes in RSNs. Neither single nor multiple spikes of any RSNs in r4–r6 elicited postsynaptic responses in the M-cell axon (Figure 12A). The lack of synaptic potentials in the M-cell axon may have been due to the electrotonic reduction of synaptic potentials during propagation from peripheral synaptic sites to the soma. However, this seemed unlikely because excitatory PSPs elicited by the stimulation of pVIIIn (n = 40, data not shown) or the posterior lateral line nerve (n = 34, data not shown) in a distal lateral dendrite of the M-cell could be detected in the axon and the soma of the M-cell. This was confirmed by the recordings in the M-cell soma, which showed no voltage changes elicited by firing of MiD2i (Figure 12B) or MiV2 cells. Therefore, we concluded that there were no apparent connections from RSNs in r4–r6 to the M-cell and that functional connections between them were unidirectional from the M-cell to RSNs in r4–r6.

Discussion

It was demonstrated that there were unidirectional connections from the M-cell to RSNs in r4–r6: Dorsally located MiD cells except for MiD2cm receive inhibitory inputs on the ipsilateral side but excitatory inputs on the contralateral side from the M-cell while ventrally located MiV cells receive equally strong excitatory inputs from the M-cell on both sides (Figure, 13A). These connections were cell-specific and repeated in r4 to r6 segments. The inhibitions derived from the ipsilateral M-cell were effective enough to shutoff ongoing spike activities in MiD cells while excitations from the M-cell enhanced the activities of contralateral MiD cells and bilateral MiV cells. These data show a functional hierarchy from the M-cell to RSNs in r4–r6 segmental homologous

RSNs: activities of RSNs might be under control of the M-cell.

Interneurons mediating between the M-cell and RSNs in r4–r6

M-cells are excitatory neurons, since activation of these cells produce monosynaptic EPSPs in cranial relay neurons in the hindbrain (Hackett and Faber, 1983a; Hackett and Buchheim, 1984), motoneurons and interneurons in the spinal cord (Fetcho and Faber, 1988). There was no apparent morphological connection between the M-cell and RSNs (Chapter 1). The onset latencies from the M-cell to the RSNs were more than about 1 ms (Chapter 2). From these observations, interneurons must be mediated between the M-cell and RSNs. Similar shapes of PSPs elicited in each group of RSNs by the M-cell spiking suggest that similar interneurons specific for each group are interposed between them. Because IPSPs from the M-cell to ipsilateral MiD cells were blocked by strychnine (Figure 7B), interneurons were possibly glycinergic neurons involved in stripes that extending rostrocaudally throughout the hindbrain as in larval zebrafish (Kinkhabwala et al., 2011). The interneurons between the M-cell and RSNs, presumably including glycinergic McCoLA (Moly and Hatta, 2011) and cranial relay neurons (T interneurons in zebrafish) (Hackett and Faber, 1983a, b; Hackett and Buchheim, 1984; Kimmel et al., 1985; Waldeck et al., 2000; Koyama et al., 2011), remain to be identified to elucidate complete circuits for the M-cell-triggered behaviors.

Different roles in the control of escape behaviors between dorsal and ventral hindbrain RSNs

Goldfish C-start escape consists of a fast C-shaped body bend (C-bend) during the initial 15–40 ms at stage 1 and a subsequent forward propulsion, which is accompanied

by a direction change in stage 2, producing a wide range of escape trajectories (Figure 13B) (Eaton et al., 1988; Foreman and Eaton, 1993). For sound-evoked C-start, a single M-cell spike is associated with initiation of C-bend to the contralateral side (Zottoli, 1977; Eaton et al., 1981; Kohashi and Oda, 2008). Activities of MiD cells, which also receive excitatory inputs from auditory nerve (Nakayama and Oda, 2004), and MiV cells, which do not receive strong auditory inputs as MiD cells (unpublished observation), are strongly modified by M-cell firing. Considering the time lag between firing of RSNs and escape behavior (8 ms in the case of M-cell, Weiss et al., 2006), the time course of PSPs and resulting firing of RSNs evoked by M-cell suggest functional roles of RSNs in control of the different motions of M-cell-initiated escape, such as C-bend, forward propulsion, and direction change. The multiunit recordings in hindbrain from the descending axons of the brainstem escape network, which includes the homologs, predict whether or not there is a direction change (Weiss et al., 2006). The M-cell connectivity with dorsally located RSNs, as shown in the present study, suggests that a single M-cell spiking suppresses activity in ipsilateral MiD cells for 10–50 ms and enhances activity in contralateral MiD cells for approximately 10 ms during stage 1 (Figure 13C). Asymmetric M-cell output onto bilateral MiM1D in r4 and MiD cells in r5 and r6, except for MiD2cm, may contribute to the lateralized spinal cord neuron activation to trigger fast trunk C-bend during stage 1 (Figure 13C). In zebrafish, backfilling and transgenic labeling studies has suggested that contralaterally projecting MiD2cm and MiD3cm are glycinergic (Barreiro-Iglesias et al., 2013; Moly et al., 2014) and ipsilaterally projecting MiDi cells are glutamatergic (Kinkhabwala et al., 2011; Kimura et al., 2013). If this is the case in goldfish, inhibitory M-cell effects on ipsilateral MiDi and MiD3cm cells may disfacilitate ipsilateral spinal neurons but disinhibit

contralateral neurons, respectively. In contrast, excitatory effects on contralateral MiDi and MiD3cm cells may excite contralateral spinal neurons and inhibit ipsilateral neurons, respectively, enhancing the lateralized activity of spinal cord neurons. Rebound activity of ipsilateral MiD cells followed by IPSPs may contribute to body stretching (or counterturn in zebrafish) after initial C-bend. In contrast, MiD2cm cells that receive inhibitory inputs from the bilateral M-cells during stage 1, have axonal arbors that project bilaterally to the spinal cord (Gahtan and O'Malley, 2003), suggesting their involvement in bilateral motor control through disinhibition.

All MiV cells received strong bilateral excitation from the M-cell during the initial phase of stage 1. Then strong inhibition occurred from the middle of stage 1 to stage 2 in MiV1 and MiV3 cells, whereas long-lasting excitation lasted over stage 2 in MiV2 cells (Figures 11E–H, 13C). It has been shown in zebrafish that activity of MiV cells correlated to swimming rhythm (Ahrens et al., 2012; Kimura et al., 2013), and MiV cells' ablation eliminates visually induced turns toward the ablated side (Orger et al., 2008; Huang et al., 2013). MiV cells are a part of *alx*-positive neurons, which belong to the medial stripe in several glutamatergic stripes rostrocaudally distributing from the hindbrain to the spinal cord (Kinkhabwala et al., 2011). Spinal *alx* neurons provide direct excitatory signals to motorneurons in zebrafish (Kimura et al., 2006). Therefore, we assume that MiV cells may also be associated in controlling swimming in goldfish. If so, initial strong excitation may reset the bilateral swimming rhythm at stage 1 (Jayne and Lauder, 1993; Svoboda and Fetcho, 1996), and the subsequent long-lasting activity may be involved in the stage 2 propulsion force in goldfish or burst swimming in zebrafish after the M-cell-triggered C-bend. In lamprey, similar depolarizing plateau potentials in RSNs, induced by activation of non-selective cation channels, are

associated with swimming (Viana Di Prisco et al., 1997; Viana Di Prisco et al., 2000). Thus, long-lasting depolarization elicited in MiV cells may contribute to forward propulsion with or without counterturn and swimming after C-bend by sending sustained excitation to the spinal cord.

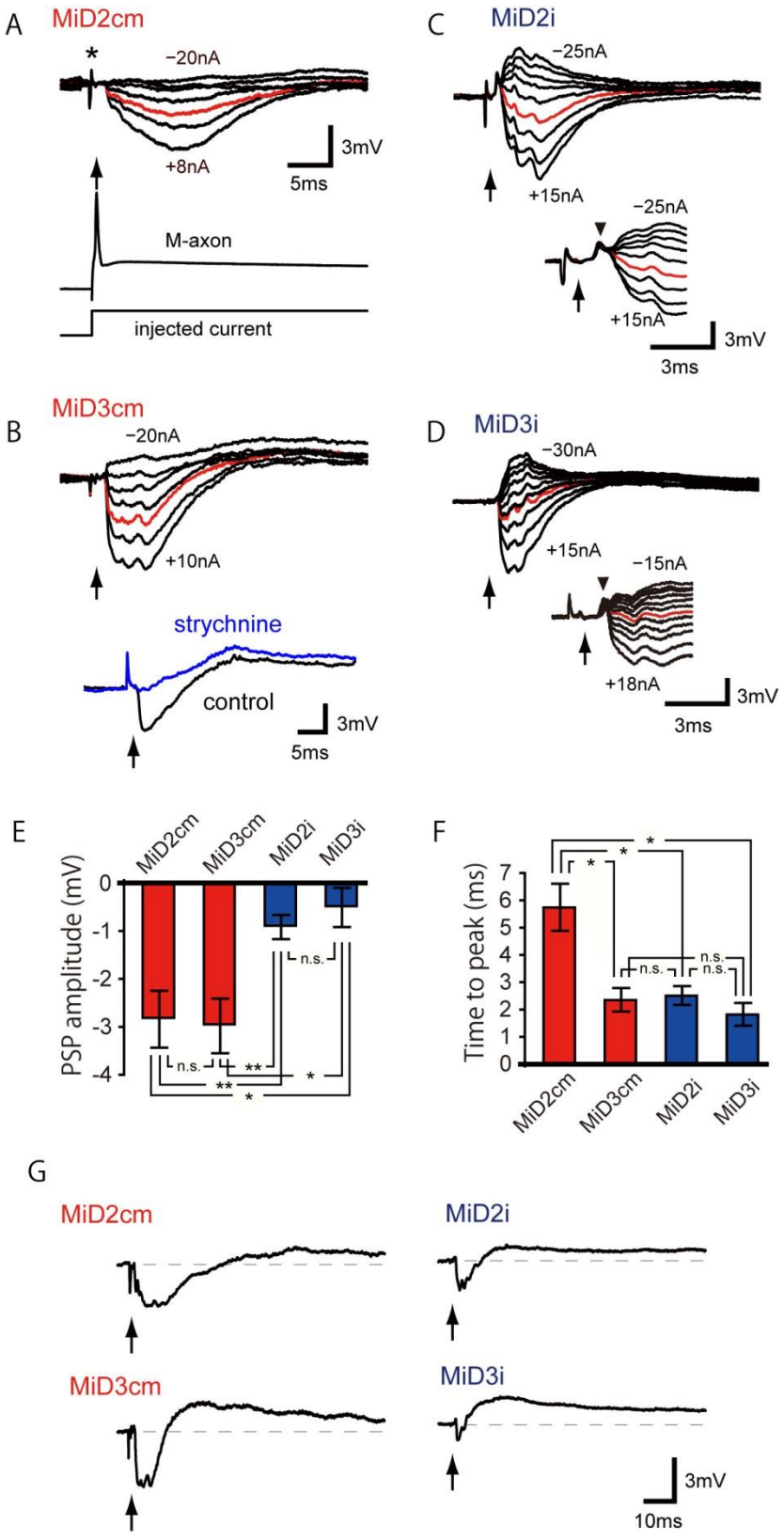
A
MiD2cm
−20nA
+8nA
3mV
5ms
M-axon
injected current
C
MiD2i
−25nA
+15nA
−25nA
+15nA
3mV
3ms
B
MiD3cm
−20nA
+10nA
strychnine
control
3mV
5ms
D
MiD3i
−30nA
+15nA
−15nA
+18nA
3mV
3ms
E
PSP amplitude (mV)
MiD2cm
MiD3cm
MiD2i
MiD3i
n.s.
**
*
F
Time to peak (ms)
n.s.
G
MiD2cm
MiD2i
MiD3cm
MiD3i
3mV
10ms

Figure 7. Ipsilateral connections from the Mauthner cell to MiD cells in r5 and r6.

Synaptic responses evoked in MiD cells by the ipsilateral M-cell firing. A–D: Intra-axonal activation of AP in the ipsilateral M-cell axon, as exemplified in the lower trace of A, and the timing of AP peak, represented by arrows (same in the following Figure 5–8), produced a small hyperpolarization (red) in MiD2cm with E_{rest} of −81 mV (A), in MiD3cm at −87 mV (B), in MiD2i at −77 mV (C), and in MiD3i at −74 mV (D). The intensities of the injected currents were increased by 5 nA, except for A wherein the currents were +8, +5, 0, −5, −10, −15, and −20 nA, and the range was denoted in nanoamperes for each cell. Note that artifact potentials caused by injecting currents into the M-axon for activation, appeared in the response traces (e.g., asterisk in A) before the spike of the M-axon (arrow) in most of the traces in Figures 5–8. Inhibitory postsynaptic potentials were blocked by applying strychnine on the remaining slow depolarizations in the MiD3cm cell (B, lower trace). In some MiD2i and MiD3i cells, sharp depolarizations were observed before IPSPs, as exemplified in the lower traces of C and D at E_{rest} of −77 mV and −91 mV, respectively (upper and lower traces were obtained in different cells in D). Amplitudes of these potentials were insensitive to the polarization of the recorded cells. E, F: Bar graphs quantifying PSP amplitudes and peak times from the onset at E_{rest}; $^{**}p < 0.01$, $^{*}p < 0.05$, n.s. not significant. G: All MiD cells showed a small long-lasting depolarization (>200 ms) after initial hyperpolarization. The calibration in A is also applicable to upper traces in B–D.

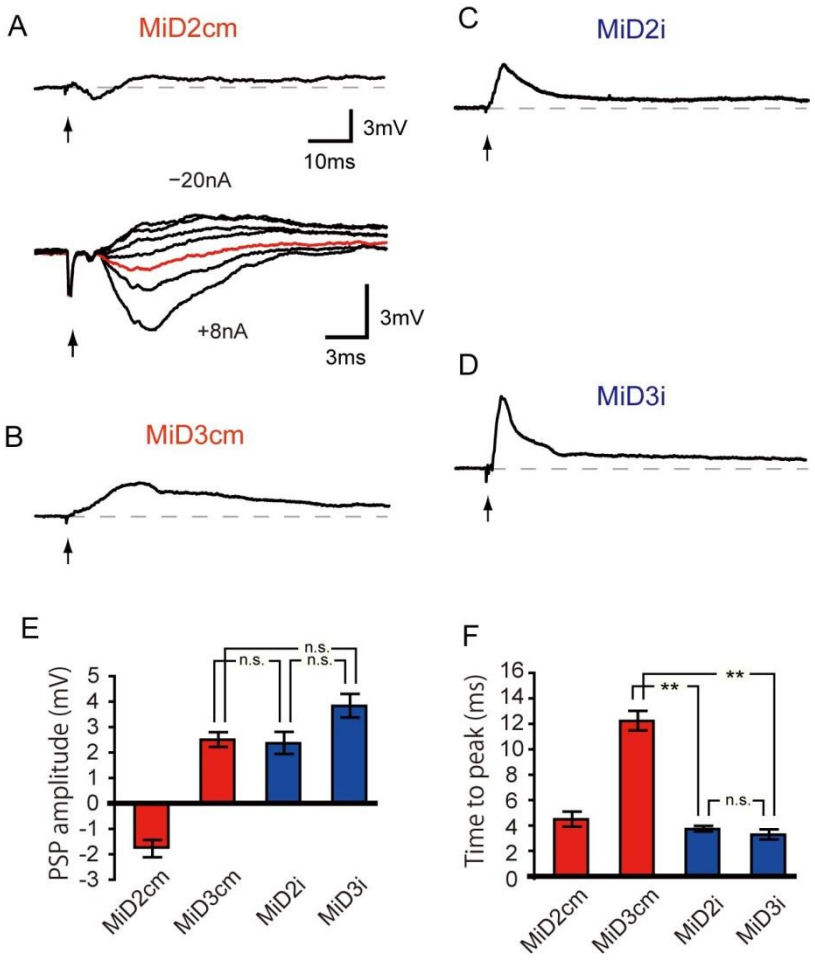

Figure 8. Contralateral connections from the Mauthner cell to MiD cells in r5 and r6. An AP of the M-cell produced long-lasting depolarization in MiD cells on the contralateral side, whereas short hyperpolarization preceded the depolarization only in MiD2cm, with E_{rest} of −80 mV for MiD2cm (A), −78 mV for MiD3cm (B), −83 mV for MiD2i (C), and −75 mV for MiD3i (D), respectively. Depolarizations evoked in MiD2i and MiD3i were similar in shape. The initial hyperpolarizing response observed in MiD2cm cell was changed in amplitude and reversed in polarity when the cell was polarized (−20, −15, −10, −5, +5, +8 nA) (A, below). Red trace is the response at E_{rest}. The calibration for upper trace of A is applicable to B, C and D. E, F: Bar graphs quantifying PSP amplitudes and peak times from the onset at E_{rest}; **$p < 0.01$, *$p < 0.05$, n.s. not significant.

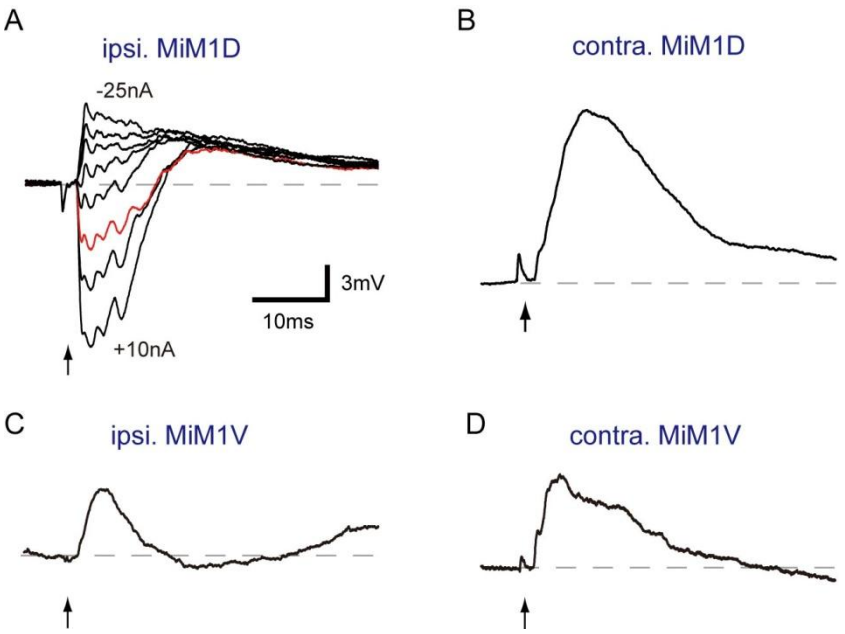

Figure 9. Subtypes of MiM1 cells receiving different inputs from the Mauthner cell. Postsynaptic responses were elicited in bilateral MiM1D and MiM1V cells by the M-cell firing. An AP of the M-cell (arrows) produced hyperpolarization, followed by depolarization with E_{rest} of −80 mV (red) in an ipsilateral MiM1D (A), whereas only depolarization was produced in a contralateral MiM1D cell at E_{rest} of −79 mV (B). The initial hyperpolarizing response observed in MiM1D cells was sensitive to the currents passing through the micropipette (−25, −20, −15, −10, −5, +5, +10 nA). C and D: Initial depolarizations at E_{rest} of −74 mV were bilaterally recorded in MiM1V cells. The calibration in A is also applicable to B–D.

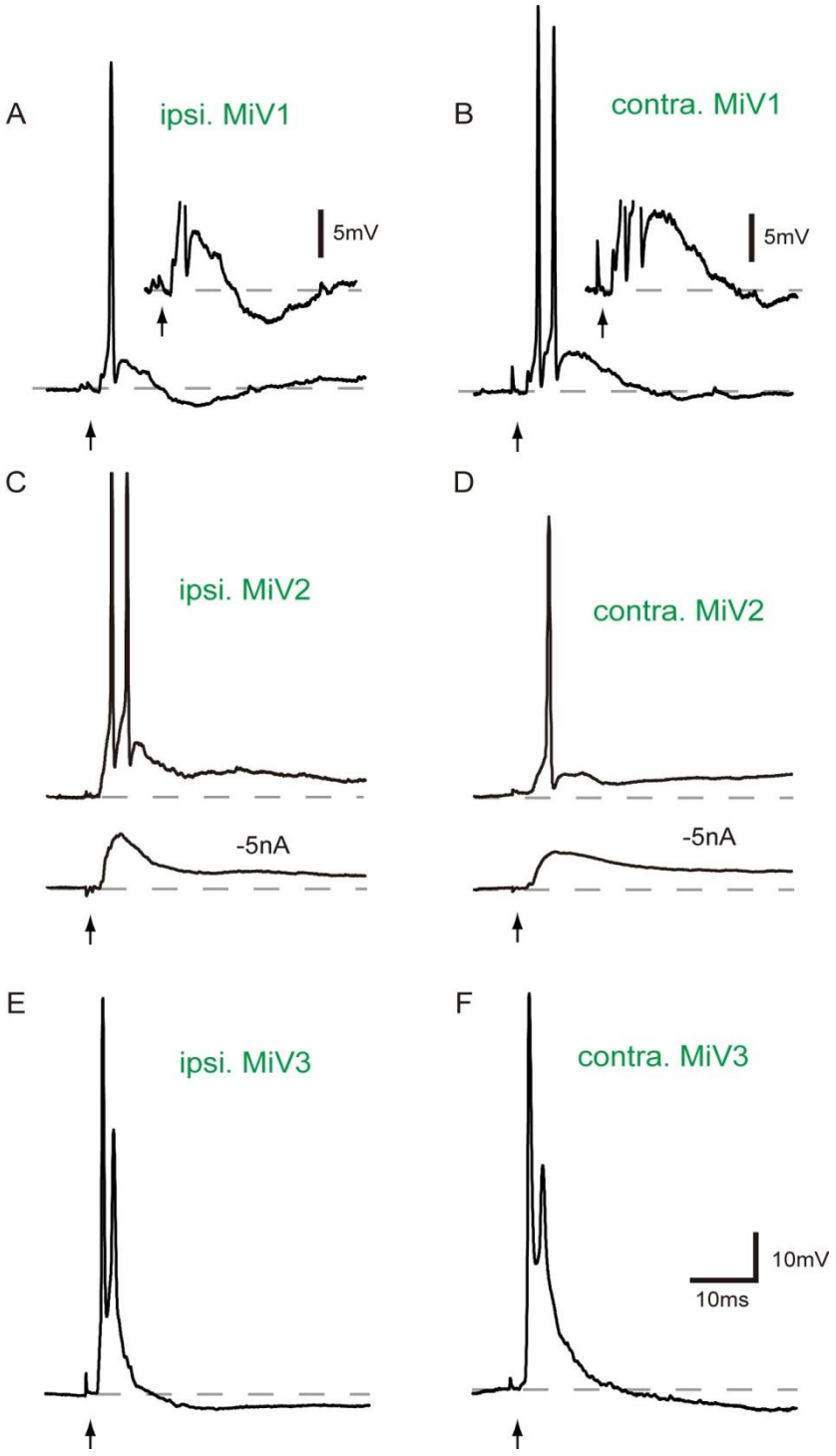
A
ipsi. MiV1
5mV
B
contra. MiV1
5mV
C
ipsi. MiV2
-5nA
D
contra. MiV2
-5nA
E
ipsi. MiV3
F
contra. MiV3
10mV
10ms

Figure 10. Strong excitatory outputs from the Mauthner cell to bilateral MiV cells in r4–r6.

A–F: Activation of the M-cell (arrows) produced strong depolarizing responses with spiking in bilateral MiV1, MiV2, and MiV3 cells (A, C, E, ipsilateral; B, D, F, contralateral). APs were followed by hyperpolarization in bilateral MiV1 (enlarged insets in A and B with calibration of 5 mV) and MiV3 cells, whereas long-lasting depolarizations were observed in bilateral MiV2 cells. E_{rest} were −71 mV in A, −82 mV in B, −73 mV in C, −76 mV in D, −74 mV in E, and −81 mV in F. Underlying depolarizing potentials were shown by hyperpolarizing the cell (−5 nA) in lower traces of C and D. The calibration in F is also applicable to A–E.

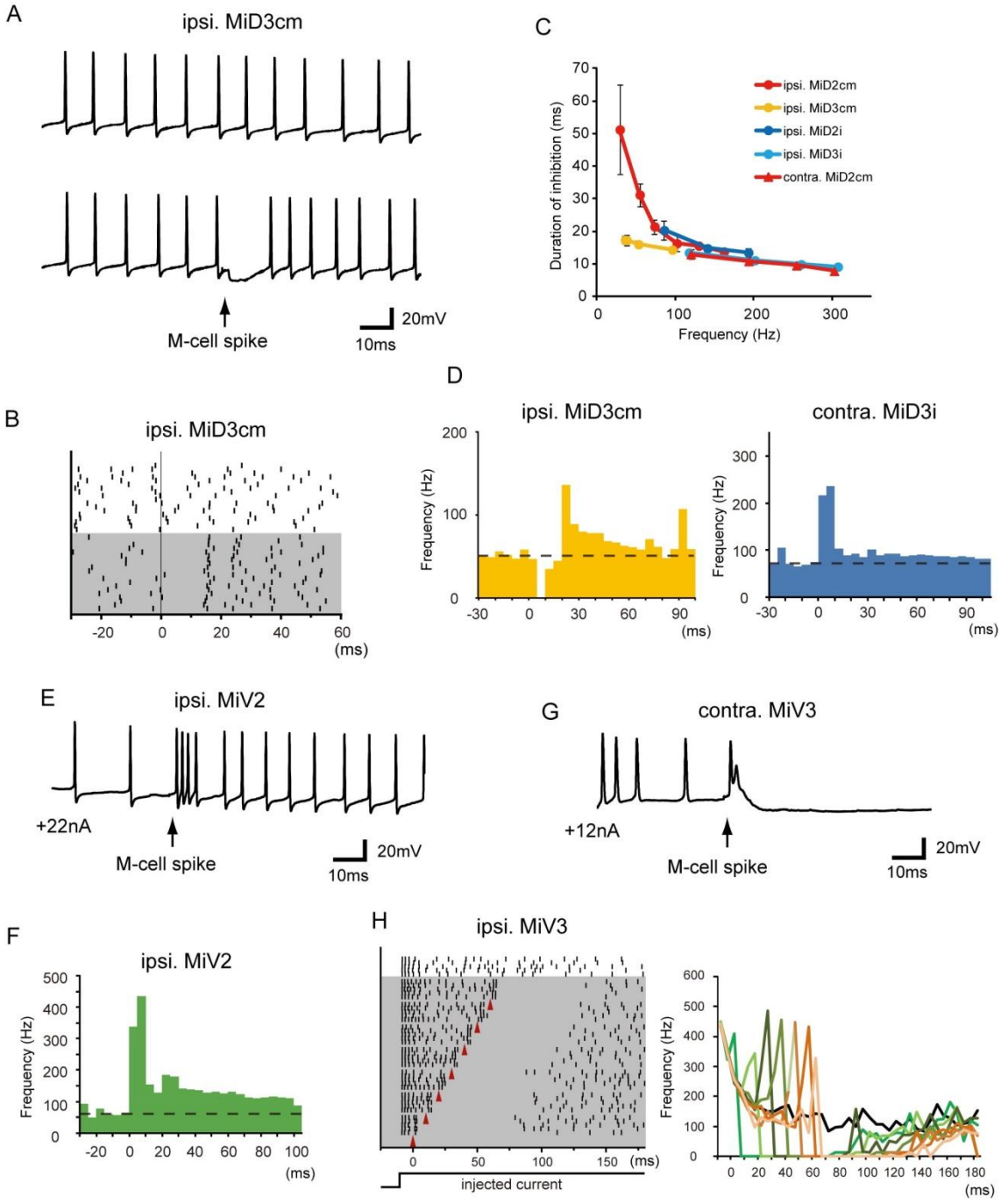
A
ipsi. MiD3cm
M-cell spike
20mV
10ms
C
ipsi. MiD2cm
ipsi. MiD3cm
ipsi. MiD2i
ipsi. MiD3i
contra. MiD2cm
Duration of inhibition (ms)
Frequency (Hz)
B
ipsi. MiD3cm
(ms)
D
ipsi. MiD3cm
contra. MiD3i
Frequency (Hz)
(ms)
E
ipsi. MiV2
+22nA
M-cell spike
20mV
10ms
G
contra. MiV3
+12nA
M-cell spike
20mV
10ms
F
ipsi. MiV2
Frequency (Hz)
(ms)
H
ipsi. MiV3
injected current
Frequency (Hz)
(ms)

Figure 11. Effects of the Mauthner cell spiking on the bursting of bilateral MiD and MiV cells.

A: Repetitive firings of an MiD3cm induced by injecting depolarizing current (upper trace, +22 nA) were temporally suppressed (lower trace) after spiking of the ipsilateral M-cell (arrow). B: Raster plots showing the timing of the spikes in the MiD3cm cell shown in A without (white) and with (gray) the M-cell spike elicited at 0 ms. C: Durations of inhibition (ms) plotted against the base line firing rate (Hz; mean ± standard deviation). The numbers of responses were 18–43 in ipsilateral MiD2cm, 17–40 in ipsilateral MiD3cm, 17–28 in ipsilateral MiD2i, 16–19 in ipsilateral MiD3i, and 12–22 in contralateral MiD2cm. D: Peristimulus time histograms (PSTHs) showing the averaged frequency of each spike of an MiD3cm cell on the ipsilateral side and an MiD3i cell on the contralateral side in response to the M-cell spike elicited at 0 ms (bin size was 5 ms). Firings of the ipsilateral MiD3cm cell was temporally stopped and enhanced later by a single spike of the M-cell (40 responses), whereas transient activation was elicited in the contralateral MiD3i cell (27 responses). E: Firing of an MiV2 cell was strongly enhanced after a single spike of the ipsilateral M-cell (arrow). F: PSTH represents the average frequency of APs of an ipsilateral MiV2 cell (bin size was 5 ms, 14 responses) in response to the M-cell spike at 0 ms. G: Firings of an MiV3 cell was instantaneously enhanced when the contralateral M-cell was fired (arrow), followed by a long-lasting suppression of activity. H: Raster plots (left) showing the effects of the M-cell firing (red arrowheads in gray area) on an ipsilateral MiV3. Transient enhancements and the following suppression of spiking were observed after the M-cell firing was applied at any phase of the MiV3 firing elicited by injected step depolarizing currents (bottom). Instantaneous change in the firing frequency of the MiV3 cell for each response (right) is shown in a different color.

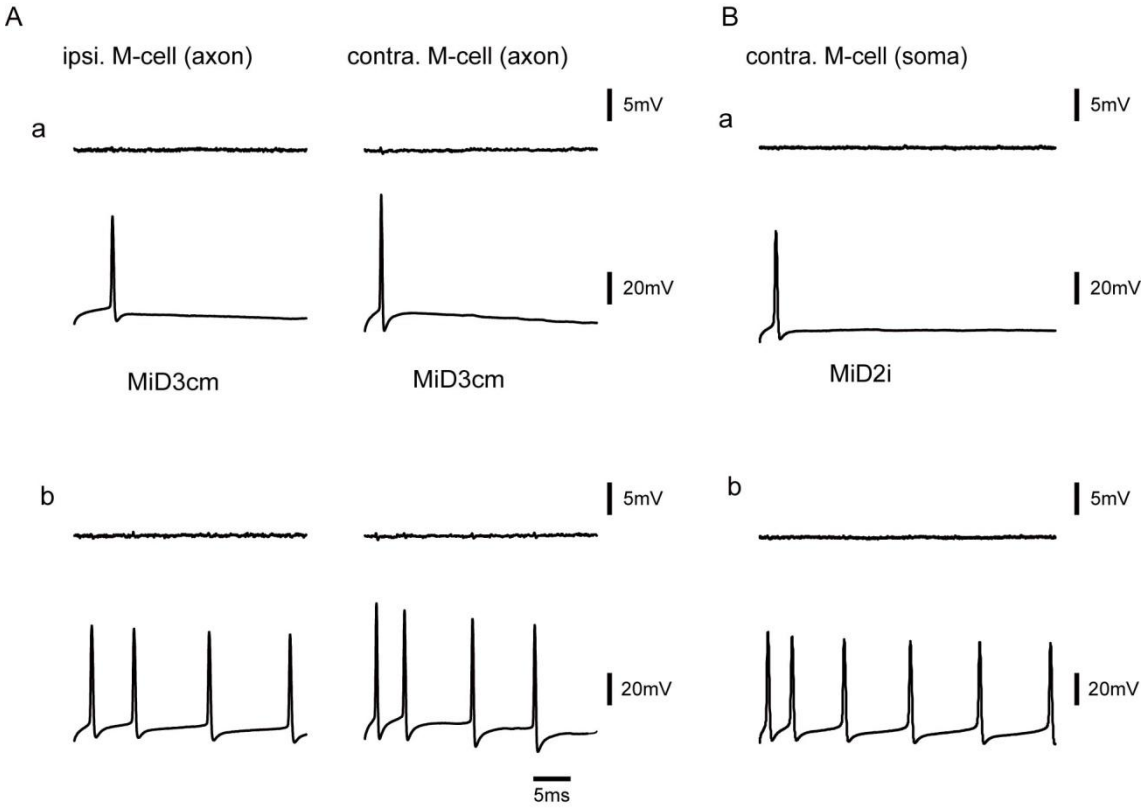

Figure 12. No inputs from RSNs to the Mauthner cell.

A: A single (a) or multiple (b) spikes of MiD3cm cells (lower) induced by injecting step depolarizing currents did not elicit any apparent bilateral potential responses in the M-cell axons (upper; left, ipsilateral; right, contralateral). B: No synaptic response was observed in the soma of the M-cell after single (a) or multiple (b) spiking of a contralateral MiD2i cell.

Table 2.

Synaptic latencies from the M-cell spike to each RSN

	latencies (ms)			
	ipsilateral	n	contralateral	n
MiD2cm	1.1±0.04	6	2.0±0.05	6
MiD3cm	1.1±0.08	6	2.4±0.10	10
MiM1D	1.0±0.03	4	1.4±0.15	3
MiM1V	1.3±0.08	3	1.1±0.07	5
MiD2i	1.1±0.03	23	1.3±0.14	9
MiD3i	1.1±0.06	6	1.5±0.07	8
MiV1	1.3±0.06	4	1.2±0.10	4
MiV2	1.4±0.05	9	1.5±0.12	7
MiV3	1.0±0.03	5	0.9±0.05	8

Table 2. Synaptic latencies from the Mauthner cells spike to each RSN.
Values were measured from the peak of the M-cell spike to the onset of the synaptic potential for each RSN (means ± standard error of the mean; n = number of cells).

General Discussion

The present study has provided the first intra-brainstem circuitry that modulates the descending motor pathways (Chapter 2): unidirectional connections from the M-cell in r4 to RSNs in r4–r6 in goldfish hindbrain (Figure 13A). Further we have also provided complementary neuroanatomical information (Chapter 1), boosting the significance of this work. The common findings of both Chapter 1 and 2 are that segmentally homologous neurons are morphologically and functionally similar but have some differences. Of note, connectivity clearly depends on the morphological homology of the targets and is almost duplicated in r4–r6. The M-cell delivers bilaterally opposing inputs to dorsally located MiD and MiM1D cells, except for MiD2cm, and delivers bilateral symmetrical inputs to ventrally located MiV and MiM1V cells. These suggest that morphologically homologous RSNs share homologous connectivity with a higher neuron (M-cell) and that RSNs comprise functional modules in the hierarchically organized motor control network. Further, the present findings would support the idea that the hindbrain segments are derived from duplication and divergence and advance the understanding in functional consequences of the segmentally homologous neurons in M-cell-initiated escape behavior of fish.

Because the M-cell is thought to be cholinergic (Day et al., 1983; Hanneman et al., 1988; Hanneman and Westerfield, 1989), the M-cell neurotransmission is susceptible to bath-applied tubocurarine in zebrafish (Koyama et al., 2011). However, in goldfish, the M-cell synaptic transmission remains functional after intramuscular anesthetization with tubocurarine (Furukawa and Furshpan, 1963; Fetcho and Faber, 1988; Waldeck et al., 2000), which probably does not cross the blood–brain barrier (Cohen, 1963).

Nevertheless, goldfish hindbrain RSNs are quite similarly identified as those in zebrafish. We have determined the functional connectivity from the M-cell to RSNs in the goldfish hindbrain. Together with multidisciplinary approaches in zebrafish including such as molecular biology, genetics, imaging, optogenetics and behavioral analysis, we can better understand cellular mechanisms underlying M-cell-triggered behaviors.

Functional division of RSNs along the dorsoventral axis

The present study suggests that MiD cells contributes to C-bend during stage 1 whereas MiV cells both stage 1 and stage 2 (Chapter 2). These imply functional division of RSNs along the dorsoventral axis. In the spinal cord, which has also segmental structure, various interneurons and motor neurons that express specific transcription factors are identified along the dorsoventral axis (Higashijima et al., 2004; Kimura et al., 2006; Arber, 2012), and they are shown to be activated differently at different locomotor speed (McLean et al., 2007; Liao and Fetcho, 2008; McLean et al., 2008; Talpalar et al., 2013). Motor neurons and excitatory interneurons closest to the ventral edge of the spinal cord are active at slow swimming speeds, with progressively more dorsal cells are recruited as larvae speed up. The hindbrain functional and developmental division along the dorsoventral axis clarified in this study seems to be similar to those in the spinal cord.

To elucidate practical function of individual RSNs in C-start, fast swimming or slow swimming of zebrafish or goldfish, RSNs connectivity onto spinal neurons needs to be determined.

Segmental homology and diversity

Segmentation is one of the common principles in the formation of the central nervous system in invertebrates and vertebrates, which is controlled by segmentation genes (Schneider-Maunoury et al., 1998; Cobourne, 2000; Philippidou and Dasen, 2013). Of note, homologous neurons are observed repeatedly in adjacent segments of vertebrate hindbrain (Metcalfe et al., 1986; Clarke and Lumsden, 1993; Lee et al., 1993), spinal cord (Westerfield et al., 1986), and invertebrate ganglions (Simmons, 1977; Mittenthal and Wine, 1978; Wilson, 1979; Shafer and Calabrese, 1981; Davis, 1983; Pearson et al., 1985), suggesting common pattern formation and further functional relevance. In invertebrates, segmental homologs are known that they are derived from identical sets of precursors (Bate et al., 1981; Kramer and Weisblat, 1985) and may selectively express specific antigens, as revealed by staining with monoclonal antibodies (Zipser and McKay, 1981). These segmentally homologous neurons, however, also show segment-specific variations, for example, by adding or lacking specific morphological processes along the nerve cord (e.g. Bate et al., 1981; Gao and Macagno, 1987; Gillon and Wallace, 1984; Glover and Mason, 1986; Goodman et al., 1981; Mittenthal and Wine 1978; Shafer and Calabrese, 1981; Wilson 1979). Morphological variations among segmental homologs may reflect in part segment-specific extrinsic and intrinsic information.

In addition to repeated appearance of similar neurons in adjacent segments, intersegmental interactions may be essential for controlling coordinated movements. For instance, sectioning the hindbrain segments disrupts coordinated rhythmic activity that influences brainstem respiratory control in chick (Fortin et al., 1995; Coutinho et al., 2004), and trigeminal motorneurons in r2 and r3 innervate jaw-closers and -openers,

respectively, in zebrafish and chick (Higashijima et al., 2000; Prin et al., 2005). The present study is the first report to show neuronal organization of intersegmental interaction in vertebrates for an integrated behaviors, as suggested in invertebrate crayfish ganglion for coordinated swimming with intersegmental homologous neurons (Smarandache et al., 2009).

Our study revealed that similar connectivity motifs from the M-cell to RSNs in r4–r6 reflects the segmental homology of target RSNs. The connectivity is, however, not a perfect copy of one segment because there are some homologous modifications such as bilateral inhibition onto only MiD2cm in MiDcm cells and no inhibition after firing only in MiV2 in MiV cells. Morphological divergences are also found, such as extraordinarily large M-cells, two types MiM1 cells, and the loop-shaped axon of MiV3 cells. Similarly, functional specialization among segmentally homologous neurons occurs in locust auditory interneurons (Pearson et al., 1985) or motor neurons (Wilson and Hoyle, 1978). Further, there is fossil evidence that a Paleozoic mayfly nymph showed the homologous wing appendages, which are repeated on all thoracic and nine abdominal body segments (Kukalová-Peck, 1978). Repetition and divergence among segmental homologous neurons may be important for preadaptation to gain new functional components or acclimatize to new environments.

The next challenges are determining how these connections function during the actual M-cell-triggered escape with multiphoton imaging or optogenetic techniques in zebrafish and determining how the connectivity is modified by environment or learning and memory.

Commonality of functional organization of segments and cortical columns.

The vertical cell column of neocortex has been recognized as a functional and morphological unit (Figure 14B). The minicolumn (sometimes referred to as the microcolumn), with its 80–100 neurons, is the smallest level of vertical organization in the cortex while the macrocolumn is a larger unit that consists of many minicolumns (Buxhoeveden and Casanova, 2002). Cortical minicolumns are often considered highly repetitive, even clone-like units, seem to be similar to segments of hindbrain (Figure 14).

Mountcastle (1997) defines a macrocolumn as: 'Many minicolumns bound together by short-range horizontal connections. Neurons within a column share certain static and dynamic physiological properties, upon which other properties may be superimposed. Minicolumns are bound into columns by both cell-autonomous and secondary histogenetic influences.' The output of a macrocolumn results from tightly knit interactions between the minicolumns. No research has yet determined the capacity of minicolumns for independent activity outside the macrocolumn that they belong to. The finding in the present study that hindbrain segments work in a coordinated manner during fish escape behavior (Figure 14A) appears similar to the macrocolumn organization in neocortex. They share properties with the concept of the module. Because the brain is a product of evolution, nothing appears in a vacuum but is a modification of what preceded it. Duplication of a basic unit with divergence and modular construction of nervous tissue are considered a common feature and may be an organizing principle of nervous system, including the hindbrain segmental structure and cerebral cortex.

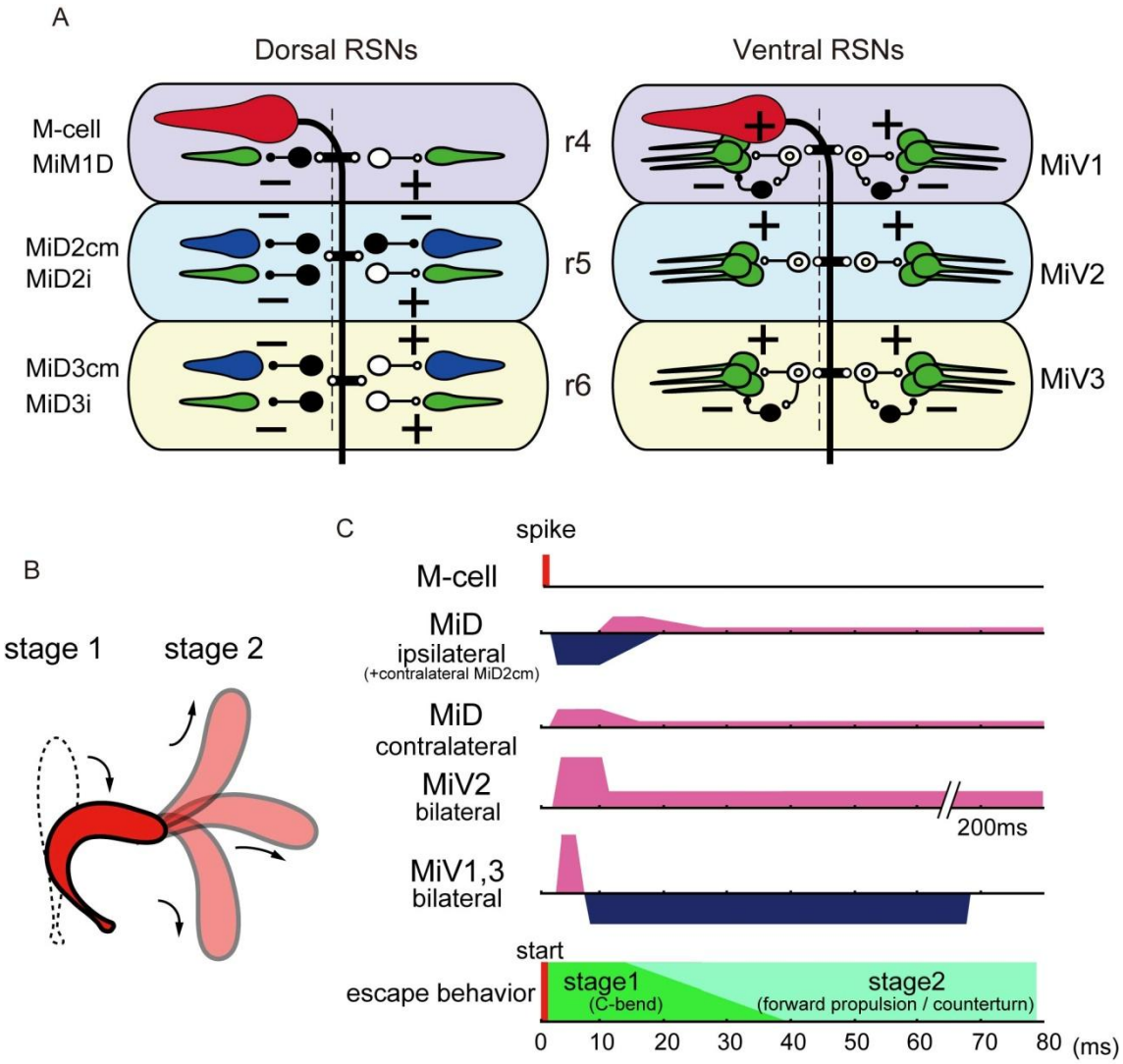
A
Dorsal RSNs
Ventral RSNs
M-cell
MiM1D
MiD2cm
MiD2i
MiD3cm
MiD3i
r4
r5
r6
MiV1
MiV2
MiV3
B
stage 1
stage 2
C
spike
M-cell
MiD
ipsilateral
(+contralateral MiD2cm)
MiD
contralateral
MiV2
bilateral
200ms
MiV1,3
bilateral
start
escape behavior
stage1
(C-bend)
stage2
(forward propulsion / counterturn)
0
10
20
30
40
50
60
70
80
(ms)

Figure 13. Escape circuitry composed of the Mauthner cell and segmentally homologous RSNs repeated in r4–r6.

A: Schematic representation of the circuits from the left M-cell to dorsally (left) and ventrally located (right) RSNs. The output of the M-cell is excitatory (possibly cholinergic, red), whereas MiD2cm and MiD3cm cells are presumably glycinergic (blue), and MiM1D, MiDi, and MiV cells are glutamatergic (green). Presumable interneurons between the M-cell and RSNs are represented as open (excitatory) and filled (inhibitory) symbols. + and −: excitatory and inhibitory synapse, respectively. B: Goldfish escape behavior. Silhouettes of C-bend at stage 1 and subsequent propelling to various directions at stage 2. C: Time course of effects of an M-cell firing on the RSNs represented on phases of C-start. The C-bend initiates about 8 ms after the M-cell activation but here, the timing of both M-cell spike and the C-bend initiation are set at 0 ms. Excitations are denoted in pink and inhibitions in blue. The duration of asymmetrical outputs from MiD cells corresponded to the stage 1 of escape, whereas that of symmetrical outputs from MiV cells lasted until stage 2.

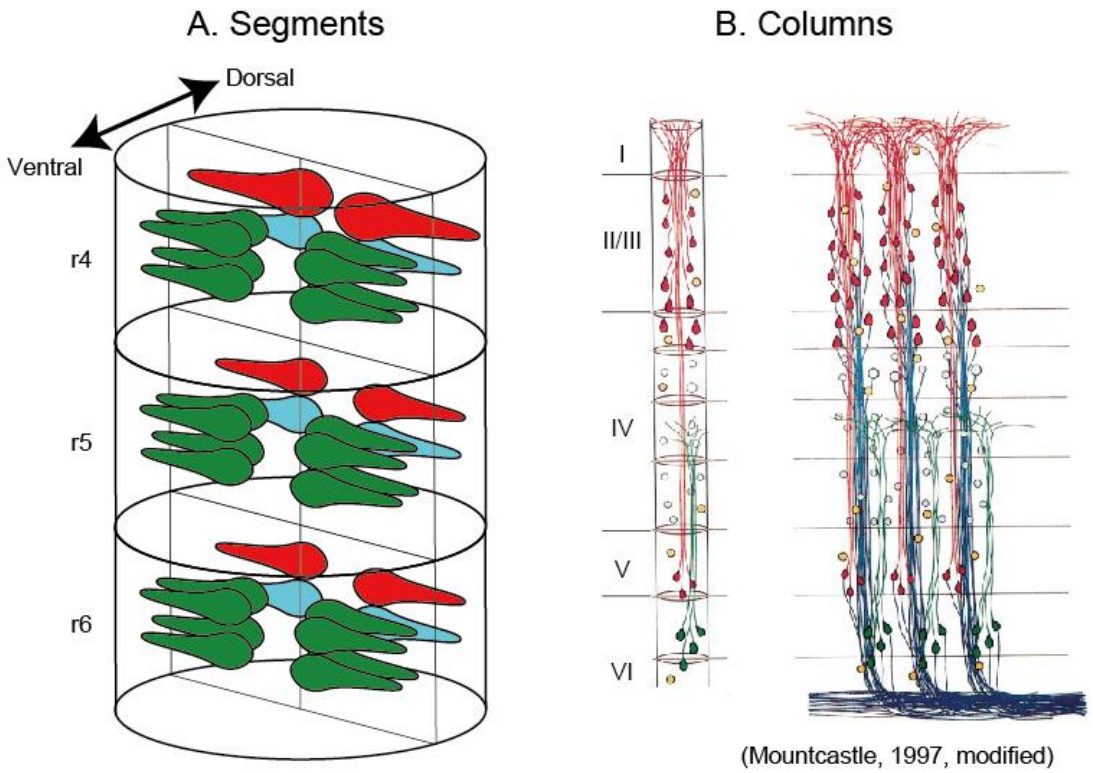

Figure 14. Diagrams of functional motifs in hindbrain segments and neocortical columns.

A. Each homologous series of RSNs repeated in r4 to r6 functions as a motif. Red and blue cells indicate dorsally located RSNs whereas green clusters are ventrally located RSNs in hindbrain.

B. Diagrams of the arrangement of neurons in vertical modules of the striate cortex of the macque monkey (from Mountcastle, 1997). Left. A drawing to show the arrangement of the pyramidal cells. Right. A drawing to represent the pyramidal columns (modules). The pyramidal cells in layers II/III, IV and V are shown in red, and those in layer VI in green.

References

Alstermark B, Isa T (2012) Circuits for skilled reaching and grasping. Annu Rev Neurosci 35:559-578.

Ahrens MB, Li JM, Orger MB, Robson DN, Schier AF, Engert F, Portugues R (2012) Brain-wide neuronal dynamics during motor adaptation in zebrafish. Nature 485:471-477.

Ahrens MB, Orger MB, Robson DN, Li JM, Keller PJ (2013) Whole-brain functional imaging at cellular resolution using light-sheet microscopy. Nat Methods 10:413-420.

Arber S (2012) Motor circuits in action: Specification, connectivity, and function. Neuron 74:975-89.

Baier H (2013) Synaptic laminae in the visual system: molecular mechanisms forming layers of perception. Annu Rev Cell Dev Biol 29:385-416.

Barreiro-Iglesias A, Mysiak KS, Adrio F, Rodicio MC, Becker CG, Becker T, Anadón R (2013) Distribution of glycinergic neurons in the brain of glycine transporter-2 Tg (glyt2:gfp) transgenic adult zebrafish: Relation with brain-spinal descending systems. J Comp Neurol 521:389-425.

Bartelmez, GW (1915) Mauthner's cell and the nucleus motorius tegmenti. J Comp Neurol 25:87-128.

Bass AH, Gilland EH, Baker R (2008) Evolutionary origins for social vocalization in a vertebrate hindbrain-spinal compartment. Science 321:417-421.

Bate M, Goodman CS, Spitzer NS (1981) Embryonic development of identified neurons: segment-specific differences in the H cell homologues. J Neurosci 1:103-106.

Buxhoeveden DP, Casanova MF (2002) The minicolumn hypothesis in neuroscience. Brain 125:935-951.

Clarke JDW, Lumsden A (1993) Segmental repetition of neuronal phenotype sets in the chick embryo hindbrain. Development 118:151-162.

Cobourne M (2000) Construction for the modern head: current concepts in craniofacial development. J Orthod 27:307-314.

Cohen EN (1963) Blood-brain barrier to *d*-tubocurarine. J Pharmacol Exp Ther 141:356-362.

Coutinho AP, Borday C, Gilthorpe J, Jungbluth S, Champagnat J, Lumsden A, Fortin G (2004) Induction of a parafacial rhythm generator by rhombomeres 3 in the chick embryo. J Neurosci 24:9383-9390.

Davis NT (1983) Serial homologies of the motor neurons of the dorsal intersegmental muscles of the cockroach, *Periplaneta Americana* (L.). J Morphol 176:197-210.

Day JW, Hall DH, Hall LM, Bennett MV (1983) α-Bungarotoxin labeling and acetylcholinesterase localization at the Mauthner fiber giant synapse in the hatchetfish. J Neurosci 3:272-279.

Deliagina TG, Beloozerova IN, Orlovsky GN (2008) Spinal and supraspinal postural networks. Brain Res Rev 57:212-221.

Eaton RC, Farley RD, Kimmel CB, Schabtach E (1977) Functional development in the Mauthner cell system of embryos of the zebra fish. J Neurobiol 8:151-172.

Eaton RC, Lavender WA, Wieland CM (1981) Identification of Mauthner-initiated

response patterns in goldfish: evidence from simultaneous cinematography and electrophysiology. J Comp Physiol [A] 144:521-531.

Eaton RC, Lavender WA, Wieland CM (1982) Alternative neural pathways initiate fast-start responses following lesions of the Mauthner neuron in goldfish. J Comp Physiol [A] 145:485-496.

Eaton RC, DiDomenico R, Nissanov J (1988) Flexible body dynamics of the goldfish C-start: implications for reticulospinal command mechanisms. J Neurosci 8:2758-2768.

Faber DS, Fetcho JR, Korn H (1989) Neuronal networks underlying the escape response in goldfish. General implications for motor control. Ann N Y Acad Sci 563:11-33.

Fetcho JR, Faber DS (1988) Identification of motoneurons and interneurons in the spinal network for escapes inhibited by the Mauthner cell in goldfish. J Neurosci 8:4192-4213.

Fetcho JR, McLean FL (2010) Some principles of organization of spinal neurons underlying locomotion in zebrafish and their implications. Ann N Y Acad Sci 1198:94-104.

Foreman MB, Eaton RC (1993) The direction change concept for reticulospinal control of goldfish escape. J Neurosci 13:4101-4113.

Fortin G, Kato F, Lumsden A, Champagnat, J (1995) Rhythm generation in the segmented hindbrain of chick embryos. J Physiol 486:735-744.

Fraser S, Keynes R, Lumsden A (1990) Segmentation in the chick embryo hindbrain is defined by cell lineage restrictions. Nature 344:431-435.

Furshpan EJ, Furukawa T (1962) Intracellular and extracellular responses of the

several regions of the Mauthner cell of the goldfish. J Neurophysiol 25:732-771.

Furukawa T, Furshpan EJ (1963) Two inhibitory mechanisms in the Mauthner neurons of goldfish. J Neurophysiol 26:140-176.

Gahtan E, Sankrithi N, Campos JB, O'Malley DM (2002) Evidence for a widespread brain stem escape network in larval zebrafish. J Neurophysiol 87:608-614.

Gahtan E, O'Malley DM (2003) Visually guided injection of identified reticulospinal neurons in zebrafish: a survey of spinal arborization patterns. J Comp Neurol 459:186-200.

Gahtan E, Tanger P, Baier H (2005) Visual prey capture in larval zebrafish is controlled by identified reticulospinal neurons downstream of the tectum. J Neurosci 25:9294-9303.

Gao WQ, Macagno ER (1987) Extension and retraction of axonal projections by some developing neurons in the leech depends upon the existence of neighboring homologues. II. The AP and AE neurons. J Neurobiol 18:295-313.

Gillon JW, Wallace BG (1984) Segmental variation in the arborization of identified neurons in the leech central nervous system. J Comp Neurol 228:142-148.

Glover JC, Mason A (1986) Morphogenesis of an identified leech neuron: segmental specification of axonal outgrowth. Dev Biol 115:256-260.

Goodman CS, Bate M, Spitzer NC (1981) Embryonic development of identified neurons: origin and transformation of the H cell. J Neurosci 1:94-102.

Greenwood AK, Peichel CL, Zottoli SJ (2009) Distinct startle responses are associated with neuroanatomical differences in pufferfishes. J Exp Biol 213:613-620.

Grillner S Jessell TM (2009) Measured motion: searching for simplicity in spinal locomotor networks. Curr Opin Neurobiol 19:572-586.

Hackett JT, Faber DS (1983a) Mauthner axon networks mediating supraspinal components of the startle response in the goldfish. Neuroscience 8:317-331.

Hackett JT, Faber DS (1983b) Relay neurons mediate collateral inhibition of the goldfish Mauthner cell. Brain Res 264:302-306.

Hackett JT, Buchheim A (1984) Ultrastructural correlates of electrical-chemical synaptic transmission in goldfish cranial motor nuclei. J Comp Neurol 224:425-436.

Hackett JT, Greenfield LJ (1986) The behavioral role of the Mauthner neuron impulse. Behav and Brain Science 9:729-730.

Hanneman E, Trevarrow B, Metcalfe WK, Kimmel CB, Westerfield M (1988) Segmental pattern of development of the hindbrain and spinal cord of the zebrafish embryo. Development 103:49-58.

Hanneman E, Westerfield M (1989) Early expression of acetylcholinesterase activity in functionally distinct neurons of the zebrafish. J Comp Neurol 284:350-361.

Heyman I, Faissner A, Lumsden A (1995) Cell and matrix specializations of rhombomere boundaries. Dev Dyn 204:301-315.

Higashijima S, Hotta Y, Okamoto H (2000) Visualization of cranial motor neurons in live transgenic zebrafish expressing green fluorescent protein under the control of the *Islet-1* promoter/enhancer. J Neurosci 20:206-218.

Higashijima S, Masino MA, Mandel G, Fetcho JR (2004) Engrailed-1 expression marks

a primitive class of inhibitory spinal interneuron. J Neurosci 24:5827-5839.

Huang KH, Ahrens MB, Dunn TW, Engert F (2013) Spinal projection neurons control turning behaviors in zebrafish. Curr Biol 23:1566-1573.

Hubel DH, Wiesel TN (1962) Receptive fields, binocular interaction and functional architecture in the cat's visual cortex. J Physiol 160:106-154.

Jayne BC, Lauder GV (1993) Red and white muscle activity and kinematics of the escape response of the bluegill sunfish during swimming. J Comp Physiol A 173:495-508.

Kiehn O (2006) Locomotor circuits in the mammalian spinal cord. Annu Rev Neurosci 29:279-306.

Kimmel CB, Powell SL, Metcalfe WK (1982) Brain neurons which project to the spinal cord in young larvae of the zebrafish. J Comp Neurol 205:112-127.

Kimmel CB, Metcalfe WK, Schabtach E (1985) T reticular interneurons: A class of serially repeating cells in the zebrafish hindbrain. J Comp Neurol 233:365-376.

Kimura Y, Okamura Y, Higashijima S (2006) alx, a zebrafish homolog of Chx10, marks ipsilateral descending excitatory interneurons that participate in the regulation of spinal locomotor circuits. J Neurosci 26:5684-5697.

Kimura Y, Satou C, Fujioka S, Shoji W, Umeda K, Ishizuka T, Yawo H, Higashijima S (2013) Hindbrain V2a neurons in the excitation of spinal locomotor circuits during zebrafish swimming. Curr Biol 23:843-849.

Kinkhabwala A, Riley M, Koyama M, Monen J, Satou C, Kimura Y, Higashijima S, Fetcho J (2011) A structural and functional ground plan for neurons in the hindbrain of

zebrafish. Proc Natl Acad Sci USA 108:1164-1169.

Kohashi T, Oda Y (2008) Initiation of Mauthner- or non-Mauthner-mediated fast escape evoked by different modes of sensory input. J Neurosci 28:10641-10653.

Koyama M, Kinkhabwala A, Satou C, Higashijima S, Fetcho J (2011) Mapping a sensory-motor network onto a structural and functional ground plan in the hindbrain. Proc Natl Acad Sci USA 108:1170-1175.

Kramer AP, Weisblat DA (1985) Developmental neural kinship groups in the leech. J Neurosci 5:388-407.

Kukalova-Peck J (1978) Origin and evolution of insect wings and their relation to metamorphosis, ad documented by the fossil record. J Morphol 156:53-126.

Lee RK, Eaton RC (1991) Identifiable reticulospinal neurons of the adult zebrafish, *Brachydanio rerio*. J Comp Neurol 304:34-52.

Lee RK, Eaton RC, Zottoli SJ (1993) Segmental arrangement of reticulospinal neurons in the goldfish hindbrain. J Comp Neurol 329:539-556.

Leise EM (1990) Modular construction of nervous systems: a basic principle of design for invertebrates and vertebrates. Brain Res Rev 15:1-23.

Liao JC, Fetcho JR (2008) Shared versus specialized glycinergic spinal interneurons in axial motor circuits of larval zebrafish. J Neurosci 28:12982-12992.

Liu KS, Fetcho JR (1999) Laser ablations reveal functional relationships of segmental hindbrain neurons in zebrafish. Neuron 23:325-335.

Lumsden A, Keynes R (1989) Segmental patterns of neuronal development in the chick

hindbrain. Nature 337:424-428.

McLean DL, Fan J, Higashijima S, Hale ME, Fetcho JR (2007) A topographic map of recruitment in spinal cord. Nature 446:71-75.

McLean DL, Masino MA, Koh IY, Lindquist WB, Fetcho JR (2008) Continuous shifts in the active set of spinal interneurons during changes in locomotor speed. Nat Neurosci 11:1419-1429.

Mendelson B (1986a) Development of reticulospinal neurons of the zebrafish. I. Time of origin. J Comp Neurol 251:160-171.

Mendelson B (1986b) Development of reticulospinal neurons of the zebrafish. II. Early axonal outgrowth and cell body position. J Comp Neurol 251:172-184.

Metcalfe WK, Mendelson B, Kimmel CB (1986) Segmental homologies among reticulospinal neurons in the hindbrain of the zebrafish larva. J Comp Neurol 251:147-159.

Mittenthal JE, Wine JJ (1978) Segmental homology and variation in flexor motoneurons of the crayfish abdomen. J Comp Neurol 177:311-334.

Moly PK, Hatta K (2011) Early glycinergic axon contact with the Mauthner neuron during zebrafish development. Neruosci Res 70:251-259.

Moly PK, Ikenaga T, Kamihagi C, Islam AF, HattaK (2014) Identification of initially appearing glycine-immunoreactive neurons in the embryonic zebrafish brain. Dev Neurobiol (in press).

Mori K, Takahashi YK, Igarashi KM, Yamaguchi M (2006) Maps of odorant molecular features in the mammalian olfactory bulb. Physiol Rev 86:409-433.

Mountcastle VB (1957) Modality and topographic properties of single neurons of cat's somatic sensory cortex. J Neurophysiol 20:408-434.

Mountcastle VB (1997) The columnar organization of the neocortex. Brain 120:701-722.

Murakami Y, Pasqualetti M, Takio Y, Hirano S, Rijli FM, Kuratani S (2004) Segmental development of reticulospinal and branchiomotor neurons in lamprey: insights into the evolution of the vertebrate hindbrain. Development 131:983-995.

Nakayama H, Oda Y (2004) Common sensory inputs and differential excitability of segmentally homologous reticulospinal neurons in the hindbrain. J Neurosci 24:3199-3209.

Nissanov J, Eaton RC, DiDomenico R (1990) The motor output of the Mauthner cell, a reticulospinal command neuron. Brain Res 517:88-98.

O'Malley DM, Kao YH, Fetcho JR (1996) Imaging the functional organization of zebrafish hindbrain segments during escape behaviors. Neuron 17:1145-1155.

Orger MB, Kampff AR, Severi KE, Bollmann JH, Engert F (2008) Control of visually guided behavior by distinct populations of spinal projection neurons. Nat Neurosci 11:327-333.

Pearson KG, Boyan GS, Bastiani M, Goodman CS (1985) Heterogeneous properties of segmentally homologous interneurons in the ventral nerve cord of locusts. J Comp Neurol 233:133-145.

Perrins R, Walford A, Roberts A (2002) Sensory activation and role of inhibitory reticulospinal neurons that stop swimming in hatchling frog tadpoles. J Neurosci 22:4229-4240.

Philippidou P, Dasen JS (2013) *Hox* genes: choreographers in neural development, architects of circuit organization. Neuron 80:12-34.

Prin F, Ng KE, Thaker U, Drescher U, Guthrie S (2005) Ephrin-As play a rhombomeres-specific role in trigeminal motor axon projections in the chick embryo. Dev Biol 279:402-419.

Rubenstein JLR, Martinez S, Shimamura K, Puelles L (1994) The embryonic vertebrate forebrain: The prosomeric model. Science 266:578-580.

Sato T, Hamaoka T, Aizawa H, Hosoya T, Okamoto H (2007) Genetic single-cell mosaic analysis implicates ephrinB2 reverse signaling in projections from the posterior tectum to the hindbrain in zebrafish. J Neurosci 27:5271-5279.

Satou C, Kimura Y, Kohashi T, Horikawa K, Takeda H, Oda Y, Higashijima S (2009) Functional role of a specialized class of spinal commissural inhibitory neurons during fast escapes in zebrafish. J Neurosci 29:6780-6793.

Schepens B, Drew T (2004) Independent and convergent signals from the pontomedullary reticular formation contribute to the control of posture and movement during reaching in the cat. J Neurophysiol 92:2217-2238.

Schepens B, Drew T (2006) Descending signals from the pontomedullary reticular formation are bilateral, asymmetric, and gated during reaching movements in the cat. J Neurophysiol 96:2229-2252.

Schneider-Maunoury S, Gilardi-Hebenstreit P, Charnay P (1998) How to build a vertebrate hindbrain. Lessons from genetics. C R Acad Sci III 321:819-834.

Shafer MR, Calabrese RL (1981) Similarities and differences in the structure of

segmentally homologous neurons that control the hearts in the leech, Hirudo medicinalis. Cell Tissue Res 214:137-153.

Sharma SC, Dunn-Meynell AA, Kobylack MA (1985) A note on a tectal neuron projecting via the tectobulbar tract in telesots. Neurosci Lett 59:265-270.

Simmons P (1977) The neuronal control of dragonfly flight I. Anatomy. J Exp Biol 71:123-140.

Smarandache C, Hall WM, Mulloney B (2009) Coordination of rhythmic motor activity by gradients of synaptic strength in a neural circuit that couples modular neural oscillators. J Neurosci 29:9351-9360.

Strausfeld NJ (2009) Brain organization and the origin of insects: an assessment. Proc R Soc B 276:1929-1937.

Supèr H, Soriano E, Uylings HBM (1998) The functions of the preplate in development and evolution of the neocortex and hippocampus. Brain Res Rev 27:40-64.

Svoboda KR, Fetcho JR (1996) Interactions between the neural network for escape and swimming in goldfish. J Neurosi 16:843-852.

Takakusaki K, Shimoda N, Matsuyama K, Mori S (1994) Discharge properties of medullary reticulospinal neurons during postural changes induced by intrapontine injections of carbachol, atropine and serotonin, and their functional linkages to hindlimb motoneurons in cats. Exp Brain Res 99:361-374.

Talpalar AE, Bouvier J, Borgius L, Fortin G, Pierani A, Kiehn O (2013) Dual-mode operation of neuronal networks involved in left-right alternation. Nature 500:85-89.

Terriente J, Gerety SS, Watanabe-Asaka T, Gonzalez-Quevedo R, Wilkinson DG (2012)

Signalling from hindbrain boundaries regulates neuronal clustering that patterns neurogenesis. Development 139:2978-2987.

Thankachan S, Fuller PM, Lu J (2012) Movement- and behavioral state-dependent activity of pontine reticulospinal neurons. Neuroscience 221:125-139.

Trevarrow B, Marks DL, Kimmel CB (1990) Organization of hindbrain segments in the zebrafish embryo. Neuron 4:669-679.

Viana Di Prisco G, Pearlstein E, Robitaille R, Dubuc R (1997) Role of sensory-evoked NMDA plateau potentials in the initiation of locomotion. Science 278:1122-1125.

Viana Di Prisco G, Pearlstein E, Le Ray D, Robitaille R, Dubuc R (2000) A cellular mechanism for the transformation of a sensory input into a motor command. J Neurosci 20:8169-8176.

Voogd J, Glickstein M (1998) The anatomy of the cerebellum. Trends Neurosci 21:370-375.

Waldeck RF, Pereda A, Faber DS (2000) Properties and plasticity of paired-pulse depression at a central synapse. J Neurosci 20:5312-5320.

Watanabe T, Shimazaki T, Mishiro A, Suzuki T, Hirata H, Tanimoto M, Oda Y (2014) Coexpression of auxiliary Kvβ2 subunits with Kv1.1 channels is required for developmental acquisition of unique firing properties of zebrafish Mauthner cells. J Neurophysiol (in press).

Weiss SA, Zottoli SJ, Do SC, Faber DS, Preuss T (2006) Correlation of C-start behaviors with neural activity recorded from the hindbrain in free-swimming goldfish (*Carassius auratus*). J Exp Biol 209:4788-4801.

Westerfield M, McMurray JV, Eisen JS (1986) Identified motoneurons and their innervations of axial muscles in the zebrafish. J Neurosci 6:2267-2277.

Wilson JA, Hoyle G (1978) Serially homologous neurons as concomitants of functional specialization. Nature 274:377-379.

Wilson JA (1979) The structure and function of serially homologous leg motor neurons in the locust. I. Anatomy. J Neurobiol 10:41-65.

Yamamoto N, Kato T, Okada Y, Somiya H (2010) Somatosensory nucleus in the torus semicircularis of cyprinid teleosts. J Comp Neurol 518:2475-2502.

Zipser B, McKay R (1981) Monoclonal antibodies distinguish identifiable neurons in the leech. Nature 289:549-554.

Zottoli SJ (1977) Correlation of the startle reflex and Mauthner cell auditory responses in unrestrained goldfish. J Exp Biol 66:243-254.

Zottoli SJ, Hordes AR, Faber DS (1987) Localization of optic tectal input to the ventral dendrite of the goldfish Mauthner cell. Brain Res 401:113-121.

Acknowledgements

I am so grateful to Prof. Yoichi Oda for instruction and helpful advice and encouragement since I became the first student in the laboratory of Brain Function and Structure in April 2005. We thank Drs. Shin. Takagi, Hiroko. Bannai, Yuichi. Takeuchi, Tsunehiko. Kohashi, Masashi. Tanimoto, Takaki. Watanabe and all the other laboratory members for helpful discussion, comments, and encouragement. I am also grateful to Dr. Shin Takagi, Azusa Kamikouchi, and Shin-ichi Higashijima for kindly proofreading my doctoral thesis.

This work was supported by Grants-in-Aid for Scientific Research (KAKENHI, 17023029, 18300134, 23115508, 25115713) from the Ministry of Education, Cultures, Sports, Science, and Technology of Japan.